

Heteroclinic connections between finite-amplitude periodic orbits emerging from a codimension two singularity

T.J. Bridges¹, D.J.B. Lloyd¹, D.J. Ratliff², and P. Sprenger³

¹School of Mathematics and Physics, University of Surrey, Guildford, GU2 7XH, UK

²Department of Maths, Phys and Elec Eng, Northumbria University, Newcastle NE1 8ST, UK

³Department of Applied Mathematics, University of California at Merced, Merced, CA 95343, USA

Abstract

Heteroclinic connections between two distinct hyperbolic periodic orbits in conservative systems are important in a wide range of applications. On the other hand, it is theoretically challenging to find large amplitude connections from scratch and compute them numerically. In this paper, we use a codimension two singularity, in a family of periodic orbits, as an organizing center for the emergence of heteroclinic connections. A normal form is derived whose unfolding produces two distinct finite amplitude periodic orbits with an explicit heteroclinic connection. We also construct heteroclinic connections far from the singularity by numerical continuation, using two numerical strategies: shooting and the core-farfield decomposition. A key geometric tool in the numerics is cylindrical foliations for the stable and unstable manifolds and their intersection. We introduce a new property of heteroclinic connections – the action – and show it is an invariant along foliations, it has a jump at a surface of section, and it appears in a central way in the normal form theory. We find that the difference in asymptotic phase between minus and plus infinity is also a key property. The theory is applied to the Swift-Hohenberg equation, the nonlinear Schrödinger with fourth order dispersion, and coupled Boussinesq equations from water waves, all of which have an energy and action conservation law.

1 Introduction

Heteroclinic connections in dynamical systems are solutions that connect two distinct states and have applications in astrodynamics [20], water waves [48, 44], pattern formation [26], and nonlinear optics [3], for example. While heteroclinic orbits involving equilibria (known as EtoE fronts) or an equilibrium and a periodic orbit (known as EtoP fronts) in Hamiltonian systems are well-studied [8, 1], much less is known about periodic to periodic connections (known as PtoP fronts) especially in conservative systems. In this paper, we consider the theory and construction of heteroclinic connections between two distinct finite-amplitude periodic states in conservative systems; see Figure 1 for an example of the types of heteroclinic connections we are interested in. We present new results on the role of action, the multiplicity of connections, the computation of asymptotic phases, and introduce a normal form for the merger of two distinct *finite-amplitude* hyperbolic periodic states (referred to as a codimension two singularity herein). Unfolding the latter singularity gives explicit connections, and a strategy for finding starting points of branches of heteroclinic connections that are otherwise highly challenging to find. We develop a numerical continuation method to find a singularity, and then use a second continuation strategy to compute large-amplitude connections far from the singularity. The role of action contains several surprises including its role in the codimension two singularity, its invariance on the stable and unstable foliations, its appearance in Floquet theory, and a jump in action that appears to be intrinsic to a connection. The main application of the theory is to nonlinear waves and patterns, where these connections are fronts between two stationary or periodic traveling waves, and so x will feature as the time-like direction.

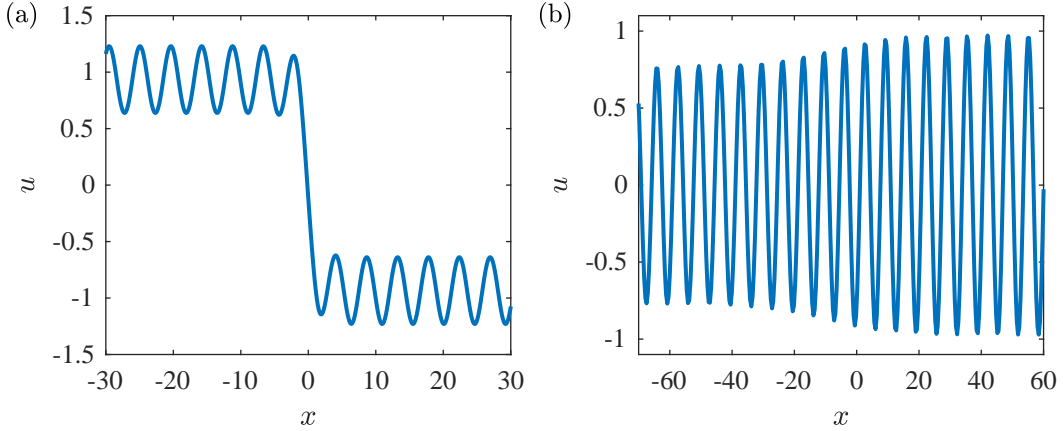


Figure 1: Examples of a heteroclinic connection between two distinct periodic states (details of this example are in §5). Panel (a) shows a heteroclinic connection between two periodic orbits in the cubic SH equation with $\sigma = 1$ and panel (b) shows a heteroclinic connection in the SH357 equation with $\mu = 0.305$, $a = 1.438$, and $b = 2.117$.

There are a range of important developments in the theory and numerics of these states in the literature that we take as starting points and build on. The geometry of these heteroclinic connections along with novel numerics has been reported in BANDARA ET AL. [4, 3, 5] as well as ZHANG ET AL. [56], using Lin’s method and a boundary-value approach. We will reproduce some of their results and extend them. The multiplicity question (how many heteroclinic connections between two fixed periodic states) has been addressed by KOON ET AL. [28] in celestial mechanics and KAHEMAN ET AL. [23] for pendulum dynamics, using shooting, and their strategy will be used here, and we add in an explicit computation of the asymptotic phases. The importance of the asymptotic phase on the periodic states at infinity is brought out in the works of BEYN [9] and DIECI & REBAZA [15] and we give a new take on this by including it in the multiplicity calculation, and taking advantage of results of PALMER [39] to aid in the computation of the stable and unstable foliations. We add to this that the action is an intrinsic invariant of the stable and unstable foliations, but jumps at a surface of section.

Effective numerical strategies that have been proposed in the literature include Lin’s Method (e.g. KRAUSKOPF & REISS [27], KNOBLOCH & REISS [27]), boundary value problems and continuation (e.g. BEYN [9], PAMPEL [40, 41], DIECI & REBAZA [15], DOEDEL ET AL. [16]), shooting (e.g. KOON ET AL. [28], BARRABÉS ET AL. [7], KAHEMAN ET AL. [23], SPRENGER [48]), pde2path for elliptic PDEs (UECKER ET AL. [53], used for heteroclinics in [26]), and the core-farfield decomposition (e.g. LLOYD & SCHEEL [30]). Our approach is to use a predictor-corrector strategy, with the shooting as predictor and the core-farfield decomposition as corrector. The shooting is effective for calculating foliations but has errors: initial data is near but not on the periodic orbit, large Floquet multipliers can lead to growth errors, and it is phase-space dimension limited. The corrector step is used to get improved accuracy. In addition to accuracy, the advantage of the core-farfield decomposition is that it extends easily to any dimension phase space, as well as to PDEs in two space dimensions.

Heteroclinic connections between periodic states are of interest in a wide range of applications: models for localised patterns with periodic tails (e.g. AOUGAB ET AL. [1], KNOBLOCH ET AL. [26]), models of optical pulses traveling down an optical waveguide with quartic dispersion (e.g. BANDARA ET AL. [4, 3, 5]), dynamics of coupled pendulums (e.g. KAHEMAN ET AL. [23]), traveling waves with oscillatory tails in the theory of nonlinear waves (e.g. SPRENGER ET AL. [48]), and the design of spacecraft trajectories in celestial mechanics (e.g. KOON ET AL. [28], WILCZAK & ZGLICZYŃSKI [54, 55], KIRCHGRABER & STOFFER [25], BARRABÉS ET AL. [7], HENRY & SCHEERES [20], SPEAR [47]).

In this paper, our examples will be the Swift-Hohenberg (SH) equation with various nonlinearities, the NLS equation with higher order dispersion (NLS4), and a coupled KdV system system from the theory of water waves. In all of these systems, the steady equation can be formulated as a Hamiltonian system. However, we will work primarily

with the equations as they arise in applications, and flag up when the symplectic geometry informs the theory.

To illustrate our strategy, consider the simplest ODE in the above class

$$u_{xxxx} + \sigma u_{xx} + V'(u) = 0, \quad (1.1)$$

for scalar-valued $u(x)$, where $V(u)$ is a given smooth nonlinear function, and σ is a real parameter. This ODE arises in the analysis of the steady SH equation, time-periodic solutions of the NLS4, and fifth-order KdV [48]. The ODE (1.1) is the Euler-Lagrange equation for the Lagrangian with density

$$L = u_x u_{xxx} + \frac{1}{2} u_{xx}^2 + \frac{1}{2} \sigma u_x^2 - V(u), \quad (1.2)$$

and energy-type function

$$H = u_x u_{xxx} - \frac{1}{2} u_{xx}^2 + \frac{1}{2} \sigma u_x^2 + V(u). \quad (1.3)$$

To avoid confusion with “free energy” (which is L in this case) in pattern formation, we will call H the Hamiltonian, even though the coordinates are not symplectic. It is a spatial Hamiltonian function as it satisfies $dH/dx = 0$, when u satisfies (1.1).

Suppose there exist two distinct periodic solutions of (1.1) of wavenumbers k^- and k^+ . Examples of a heteroclinic connection between these two states satisfying (1.1) are shown in Figure 1. As $x \rightarrow -\infty$ ($+\infty$) there is a periodic solution with a wavenumber k^- (k^+), and a core region that smoothly connects the two end states. Further details of these examples are in §5.

However, Figure 1 hides essential properties of the heteroclinic connection. Firstly, in order to match each periodic orbit to the core the correct asymptotic phase has to be computed. Secondly, there is a non-uniqueness. A pair of distinct periodic orbits on the same Hamiltonian surface can host many heteroclinic connections. We find that generically there are at least two, and there can be in principle be any finite number. The shooting strategy resolves both of these issues by computing the entire stable and unstable foliation. Computation of the foliations using shooting is carried out in a phase space representation of (1.1). Write (1.1) as a first order system following [4], with coordinates $\mathbf{u} := (u, u_x, u_{xx}, u_{xxx})$ and governing equation,

$$\mathbf{u}_x = \mathbf{f}(\mathbf{u}), \quad \mathbf{f}(\mathbf{u}) = [u_2, u_3, u_4, -\sigma u_3 - V'(u_1)]^T. \quad (1.4)$$

Although not needed at this point it is useful to note that this system is Hamiltonian with a non-canonical symplectic form

$$\mathbf{J} = \begin{bmatrix} 0 & -\sigma & 0 & -1 \\ \sigma & 0 & 1 & 0 \\ 0 & -1 & 0 & 0 \\ 1 & 0 & 0 & 0 \end{bmatrix}. \quad (1.5)$$

Multiplying (1.4) by \mathbf{J} transforms the right-hand side into ∇H , with H in (1.3) expressed in terms of the \mathbf{u} coordinates. The asymptotic phase on a hyperbolic periodic orbit is that value of θ for which

$$u(x) \rightarrow \hat{u}(z + \theta, k), \quad \text{as } x \rightarrow +\infty, \quad (1.6)$$

when $u(x)$ is initialized on the stable manifold of a periodic state, and \hat{u} is the periodic orbit

$$\hat{u}(z, k), \quad \hat{u}(z + 2\pi, k) = \hat{u}(z, k), \quad z = kx. \quad (1.7)$$

The union of all initial data that lands on a particular asymptotic phase is a leaf of the stable foliation, and the stable foliation is the union over all possible asymptotic phases. Similarly for the unstable foliation associated with the periodic state at $-\infty$.

The shooting algorithm computes the inverse of (1.6). For the stable foliation, a phase value θ^+ is fixed and integration from a large value of x back to $x = 0$ is computed, with initial data on the tangent space of the stable manifold.

Varying θ^+ then creates a cylindrical manifold which limits on a curve in the surface of section. Repeating this inverse calculation with the hyperbolic periodic orbit at $-\infty$ creates another curve in the surface of section. The transversal intersection of these two curves then provides a candidate for a heteroclinic connection. However, the situation is much more interesting as advancing the phases θ^\pm from 0 to 2π along the periodic orbit, and integrating towards the surface of section, generates a closed curve in the surface of section. To be precise, a closed curve without self-intersection, in the Poincaré section, *occurs in most of our calculations*. The exception is the case where a third periodic orbit is present on the same Hamiltonian surface and is inverse-hyperbolic, distorting the curve (see Figure 6 in §2).

A schematic of the case where we have two closed curves in the surface of section is shown in Figure 2(c). The number of intersections between these two curves gives the multiplicity of heteroclinic connections between the $\hat{u}^-(z + \theta^-, k^-)$ and $\hat{u}^+(z + \theta^+, k^+)$, and values of the phase which can be used to determine the asymptotic phases at $\pm\infty$. Figure

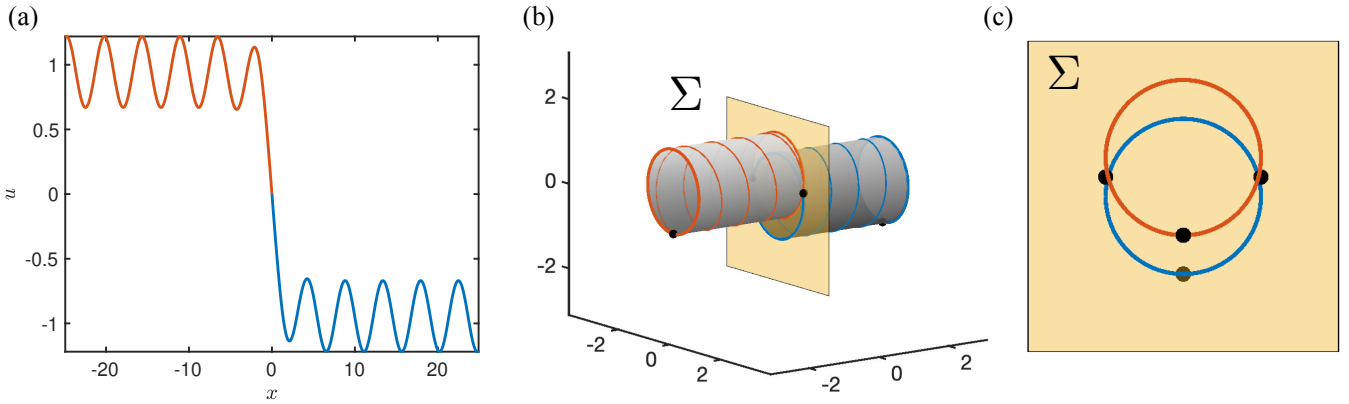


Figure 2: *Schematic of the computation of the stable and unstable foliations: panel (a) shows a heteroclinic connection associated with one of the intersection points in (c); panel (b) shows cylindrical foliations obtained by solving the inverse problem for the asymptotic phase; and panel (c) shows the surface of section at $x = 0$ illustrating the intersection between the stable (blue) and unstable (red) foliations.*

Figure 2(b) shows a schematic of the stable foliation, with a leaf in blue on the right, and the unstable foliation, with a leaf in red on the left. These two cylindrical foliations then intersect in a surface of section as shown in Figure 2(c). Figure 2(a) then shows the complete heteroclinic connection as a function of x .

Given a good approximation to a heteroclinic connection, with periodic orbits k^\pm and asymptotic phases θ^\pm , it is taken as an initial condition in the global iterative scheme of [30]. The core-farfield decomposition is a boundary-value solver, but differs from the strategy in BVP solvers in [9, 40, 41, 15, 16] in that projection boundary conditions are not used. Instead zeroth-order asymptotic boundary conditions are implemented; see §3 and Appendix A of [30] for an error analysis and convergence properties. The decomposition of the solution, using (1.1) as an example, is

$$u(x) = w(x) + \chi_+(x)\hat{u}^+(z + \theta^+, k^+) + \chi_-(x)\hat{u}^-(z + \theta^-, k^-),$$

with $w(x)$ the core solution, and smooth cut-off functions

$$\chi_\pm(x) = 1, \quad \pm x > d + 1 \quad \text{and} \quad \chi_\pm(x) = 0, \quad \pm x < d,$$

where d is a suitably-chosen large positive constant (see Figure 9 in [30]). The complete set of equations, which are then solved iteratively using Newton's method, is given in equations (2.9)–(2.13) in [30]. Numerical results are reported in §5.2 and 6.

There are two ways that the word “codimension” will be used here. First there is the codimension of the intersection of the manifolds, treated as submanifolds of the phase space and parameter space. This approach was introduced

by BEYN [9] for heteroclinic connections between periodic orbits and has been used explicitly or implicitly in all subsequent numerical studies. It identifies the number of parameters in which the solutions are generic. This codimension will be introduced in the setup of the numerics in §2. The second notion of codimension used here is the order of the singularity in parameter space of a family of periodic orbits parameterized by wavenumber.

This latter concept of codimension emerges from the normal form theory. A nonlinear normal form is derived in §4 by phase modulation of a finite-amplitude periodic state (1.7), starting with the ansatz

$$u(x) = \hat{u}(z + \varepsilon^{\rho-1}\phi, k + \varepsilon^\rho q) + \varepsilon^\mu v(z + \varepsilon^{\rho-1}\phi, X, \varepsilon), \quad X = \varepsilon^\nu x, \quad (1.8)$$

with the constraint $\phi_X = q$ and v a remainder function. The exponents ρ, μ, ν differ depending on the desired normal form. We claim that the nonlinear normal form for the wavenumber modulation has the remarkably simple form

$$\varepsilon^{2\nu+\rho} \mathcal{K} q_{XX} + A(k + \varepsilon^\rho q) = 0. \quad (1.9)$$

The function $A(k)$ is the action evaluated on a family of periodic orbits. It is a relative integral invariant, and when evaluated on periodic orbits it is

$$A(k) = \frac{d}{dk} \bar{L}_k, \quad (1.10)$$

where L is the Lagrangian (1.2), averaged on a family of periodic orbits. By defining

$$F(q) := \bar{L}(k + \varepsilon^\rho q),$$

the modulation equation is in the form of Newton's Law for a particle,

$$\varepsilon^{2\nu+2\rho} \mathcal{K} q_{XX} = -\nabla F(q),$$

with \mathcal{K} playing the role of mass. We will have other interpretations of \mathcal{K} including strategies for computing it.

At this point the form (1.9) is an assertion. We will prove it by expanding $A(k + \varepsilon^\rho q)$ in a Taylor series in ε , then use conventional phase modulation, based on the ansatz (1.8), to construct a normal form, order by order, and then prove that the coefficients are the Taylor coefficients of the action. Expanding A in a Taylor series in (1.9),

$$\varepsilon^{2\nu+\rho} \mathcal{K} q_{XX} + A(k) + A_k(k) \varepsilon^\rho q + \frac{1}{2} A_{kk}(k) \varepsilon^{2\rho} q^2 + \frac{1}{6} A_{kkk}(k) \varepsilon^{3\rho} q^3 + \dots = 0. \quad (1.11)$$

We call $A_k = 0$, for some $k \neq 0$, along a branch of periodic orbits a codimension-one singularity, and when $A_k = A_{kk} = 0$, in a two-parameter family, we call it a codimension-two singularity. This version of codimension points to the importance of plotting the action as a function of k along families of periodic orbits. A schematic of the action plotted as a function of k is in Figure 3 along with a plot of the spatial Hamiltonian of the system.

There is a close relationship between singularities in the action, and singularities in the Hamiltonian function. Evaluate the Hamiltonian function (1.3) on a family of periodic orbits of (1.1),

$$H(k) := H(\hat{u}(z, k)), \quad (1.12)$$

(using the same symbol to simplify notation). We prove in §3 that $A_k = 0$ whenever $H_k = 0$. Hence, the above codimension-two singularity occurs when

$$H_k = H_{kk} = 0, \quad \text{and} \quad H_{kkk} \neq 0. \quad (1.13)$$

The advantage of this is that the coefficients in the normal form can be also deduced, at least qualitatively, from a Hamiltonian-wavenumber diagram.

At the codimension two point the normal form, to leading order, is

$$\varepsilon^{2\nu+\rho} \mathcal{K} q_{XXX} + \frac{1}{2} A_{kkk} \varepsilon^{3\rho} q^2 q_X = 0. \quad (1.14)$$

We have differentiated the equation (1.11) as that will be the form that emerges naturally in the conventional derivation of phase modulation in §4. The terms in (1.14) are in balance when $\rho = \nu = 1$, giving

$$\mathcal{K}q_{XXX} + \frac{1}{2}A_{kkk}q^2q_X = 0. \quad (1.15)$$

Taking $\mu = 2$, the ansatz is

$$u(x) = \hat{u}(z + \phi, k + q) + \varepsilon^2 w(z + \phi, X, \varepsilon), \quad X = \varepsilon x. \quad (1.16)$$

It is straightforward to insert this ansatz into (1.1), expand all terms in Taylor series in ε and solve order by order. The solvability condition at fourth order gives a normal form like (1.15). The difficult part is then proving that the coefficients in that derivation are indeed the Taylor coefficients of the action. The proof is sketched in Appendix C, with details in the supplementary material.

A typical Hamiltonian-wavenumber diagram, which gives a starting point for finding a codimension-two point, is shown in Figure 3. There are two critical points, one a max and one a minimum, and the codimension-two point

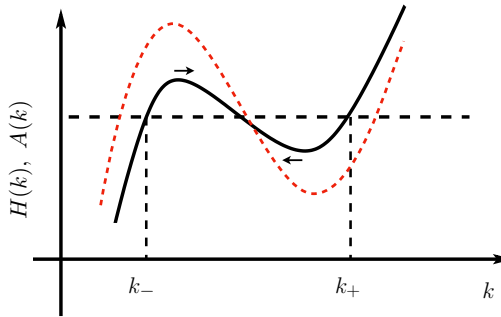


Figure 3: Plot of the value of the Hamiltonian and the Action function versus the wavenumber along a branch of periodic states near an inflection point. The solid curve corresponds to the spatial Hamiltonian and the dashed curve to the Action. Arrows indicate the motion of the critical points as the codimension 2 point is approached.

brings these two singularities together. If the branch of periodic orbits to the left of the maximum is hyperbolic, then the branch to the right of the minimum is also hyperbolic, generically, and so can be connected, if they are on the same Hamiltonian surface, and satisfy a transversality condition. Such a Hamiltonian surface can be found by drawing a horizontal line. As the codimension-two point is approached the two hyperbolic periodic orbits are close and explicit formulae for the heteroclinic connection is obtained. This graphical approach is not the only way to identify pairs of periodic orbits on the same Hamiltonian surface; indeed, since Hamiltonian surfaces are not necessarily connected, periodic orbits on different components can also be paired.

The normal form is completely integrable. The constant solutions q^\pm of (1.15) represent the periodic states at infinity, and an explicit heteroclinic exists between these two states, when \mathcal{K} and A_{kkk} have particular signs. A detailed analysis of the normal form in given in §4. The normal form theory extends to any conservative system on finite dimension. Hence the above codimension two point answers the question of how to determine if a given system has any heteroclinic connections at all: find a codimension two point and check the signs of \mathcal{K} and A_{kkk} .

We sketch the origin of the action conservation law, with details in §3. The key to action is that it is defined on an *ensemble of solutions* $u(x, s)$, with s parameterizing the ensemble. Substituting this ensemble into the Lagrangian L in (1.2) and differentiating gives the exact identity

$$L_s + u_s \left(u_{xxxx} + \sigma u_{xx} + V'(u) \right) = A_x. \quad (1.17)$$

When $u(x, s)$ is a solution (for each s), the term in brackets vanishes, and the conservation law (on ensemble space) is exact: $L_s = A_x$, with

$$A(x, s) = u_{xxx}u_s + u_x u_{xss} + \sigma u_x u_s. \quad (1.18)$$

This function, and particularly its value on families of periodic orbits, will feature prominently in the theory. Further aspects of action are developed in §3.

We will restrict attention to examples where the steady equation has a phase space of dimension four. However, much of the strategy extends to higher phase space dimension, and even to multiple space dimension (see Concluding Remarks §7).

We've chosen four example PDEs to illustrate the theory. The first equation is the Swift-Hohenberg equation

$$u_t + u_{xxxx} + \sigma u_{xx} + V'(u) = 0, \quad (1.19)$$

with polynomial $V(u)$. Two cases of SH of interest are the quadratic-cubic SH equation with

$$V(u) = \frac{1}{2}u^2 + \frac{1}{3}\nu u^3 - \frac{1}{4}u^4, \quad (1.20)$$

with ν a specified real parameter (when $\nu = 0$ it will be called the cubic SH equation), and the SH357 equation, introduced [26], where

$$V(u) = \frac{1}{2}(1-\mu)u^2 + \frac{1}{4}au^4 - \frac{1}{6}bu^6 + \frac{1}{8}u^8, \quad (1.21)$$

where a , b , and μ are real parameters (we replace λ in [26] with μ), and σ is taken to be 2 for this model. The third model is the NLS equation with fourth-order dispersion [4, 3, 5],

$$\Psi_t = i\gamma|\Psi|^2\Psi - \frac{1}{2}i\beta_2\Psi_{xx} + i\frac{\beta_4}{24}\Psi_{xxxx}, \quad (1.22)$$

where $\Psi(x, t)$ is complex-valued, and γ , β_2 , and β_4 are real-valued parameters. By taking $\Psi(x, t) = u(x)e^{i\mu t}$, it reduces to the steady equation (1.1) for the real-valued function $u(x)$, with

$$\sigma = -12\frac{\beta_2}{\beta_4} \quad \text{and} \quad V(u) = -12\frac{\mu}{\beta_4}u^2 + 6\frac{\gamma}{\beta_4}u^4. \quad (1.23)$$

In the above three models, oscillatory fronts have been found previously, and we give a new perspective and compare results. A fourth model, for which oscillatory fronts have not been previously found, is the *ac*–Boussinesq (or coupled KdV) system

$$\begin{aligned} h_t + (u + hf'(u))_x + au_{xxx} &= 0 \\ u_t + f(u)_x + gh_x + ch_{xxx} &= 0, \end{aligned} \quad (1.24)$$

where $f(u)$ is a given smooth function. The canonical case, derived from the water-wave problem, has $f(u) = \frac{1}{2}u^2$. We will extend this form by including higher order terms in f ,

$$f(u) = \frac{1}{2}u^2 + \frac{\alpha}{3}u^3, \quad (1.25)$$

for some specified parameter α . The steady system relative to the moving frame, $x \mapsto x - Ct$, is

$$\begin{aligned} ch_{xx} &= F_h \\ au_{xx} &= F_u, \end{aligned} \quad (1.26)$$

where $g > 0$ is the gravitational constant and a, c are dispersion coefficients, and

$$F(h, u) = \mathcal{A}u + \mathcal{B}h - \frac{1}{2}gh^2 - \frac{1}{2}u^2 - hf(u) + Chu, \quad (1.27)$$

where \mathcal{A}, \mathcal{B} are constants of integration. The PDE (1.26) is a model for water waves ($\alpha = 0$) and internal waves ($\alpha \neq 0$), with the coefficients a, c taking specific values (cf. BONA ET AL. [10]).

The paper is outlined as follows. In Section 2, we review the geometry of stable and unstable manifolds involved in PtoP heteroclinic orbits and explain how the asymptotic phases and multiplicity are determined. As part of the

review, we cover the recent numerics of BANDARA ET AL. [4, 3, 5] for (1.22) and reinterpret them in the context of the geometry, while also extending their result to the case where the $A \rightarrow -A$ symmetry is broken. In Section 3, we introduce the action and its link to Floquet stability analysis of spatially periodic orbits. The normal form theory is then developed in Section 4 that derives the normal form near a Hamiltonian co-dimension 2 point. We describe, in Section 5 how to find the Hamiltonian co-dimension 2 point of the periodic orbits and compute the emerging fronts for the SH357. We show in Section 6 how the theory applies to the *ac*–Boussinesq equations. Finally, we conclude in Section 7.

2 Computing foliations in the Generalized NLS Equation

In this section, we take the fourth-order NLS equation of BANDARA ET AL. [4, 3, 5] as a starting point,

$$\frac{\partial \Psi}{\partial t} = i\gamma|\Psi|^2\Psi - i\frac{\beta_2}{2}\frac{\partial^2 \Psi}{\partial x^2} + i\frac{\beta_4}{24}\frac{\partial^4 \Psi}{\partial x^4}, \quad (2.1)$$

where $\Psi(x, t)$ is complex and the parameters β_2 , β_4 , and γ are real. We have replaced coordinates A and (z, t) in [4, 3, 5] with Ψ and (t, x) to correspond with notation in this paper.

The aim of this section is three-fold. Firstly, to implement the algorithm for the cylindrical foliations depicted in Figure 2 and illustrate the use of $H - k$ and $A - k$ diagrams. Secondly, to compare with previous work in [4, 3, 5], and thirdly to show some new computations of heteroclinic connections which break the $\Psi \mapsto -\Psi$ symmetry in (2.1). We do not find a codimension two point in this example; that will come later when we add a higher order nonlinearity.

To reduce (2.1) to a steady problem, time-periodic solutions of the form $\Psi(x, t) = u(x)e^{i\mu t}$ are sought, reducing (2.1) to an ODE for $u(x)$,

$$\frac{\beta_4}{24}\frac{d^4 u}{dx^4} - \frac{\beta_2}{2}\frac{d^2 u}{dx^2} - \mu u + \gamma u^3 = 0. \quad (2.2)$$

For the cases of interest here, we take parameter values from the papers [4, 3, 5]: $\beta_4 = -1$, $\mu = \gamma = 1$. With these values, and a scaling of x , the ODE (2.2) is reduced to the form in (1.1) with $V'(u) = u - u^3$,

$$u_{xxxx} + \sigma u_{xx} + u - u^3 = 0 \quad \text{with} \quad \sigma = \beta_2\sqrt{6}. \quad (2.3)$$

Periodic orbits are denoted by $\hat{u}(z, k)$ and they satisfy the ODE,

$$k^4\hat{u}_{zzzz} + \sigma k^2\hat{u}_{zz} + \hat{u} - \hat{u}^3 = 0. \quad (2.4)$$

We consider two cases. Firstly, we look at solutions which have the $u \mapsto -u$ symmetry in §2.1. In this case the two period orbits are symmetry-related orbits. Secondly, we look at solutions that break this symmetry: either by choosing distinct periodic orbits, in §2.2, or by adding an explicit symmetry breaking term in the nonlinearity, in §2.3.

2.1 Connecting symmetry-related periodic orbits

This case gives a clear illustration of the cylindrical foliations of the stable and unstable manifolds, as well as the calculation of the asymptotic phase and the multiplicity count. For the states at infinity we compute one family of periodic orbits, $\hat{u}(z, k)$ then the other is just minus this, $-\hat{u}(z, k)$.

For simplicity, take $\sigma = 1$, and look for periodic solutions bifurcating from the constant states $u = \pm 1$. Linearizing (2.3) about these constant states and looking for normal mode solutions e^{ikx} , with $\sigma = 1$, gives the characteristic equation

$$k^4 - k^2 - 2 = 0. \quad (2.5)$$

The only positive real root is $k = \sqrt{2}$. There exists a pair of periodic orbits, $\hat{u}^\pm(z, k^\pm)$, parameterized by k , related by symmetry

$$\hat{u}^-(z, k^-) = -\hat{u}^+(z, k^+) := -\hat{u}(z, k), \quad k^+ = k^- := k,$$

and bifurcating from the constant solutions with $k = \sqrt{2}$. The Hamiltonian and action functions along the branch of periodic orbits are

$$H = k^4 \hat{u}_z \hat{u}_{zzz} - \frac{1}{2} k^4 \hat{u}_{zz}^2 + \frac{1}{2} k^2 \hat{u}_z^2 + \frac{1}{2} \hat{u}^2 - \frac{1}{4} \hat{u}^4 \quad \text{and} \quad A = \frac{1}{2\pi} \int_0^{2\pi} (\sigma k \hat{u}_z^2 - k^3 \hat{u}_{zz}^2) dz,$$

and they are plotted along the branch in Figure 4. The starting point in Figure 4 is on the right where $k = \sqrt{2}$ and

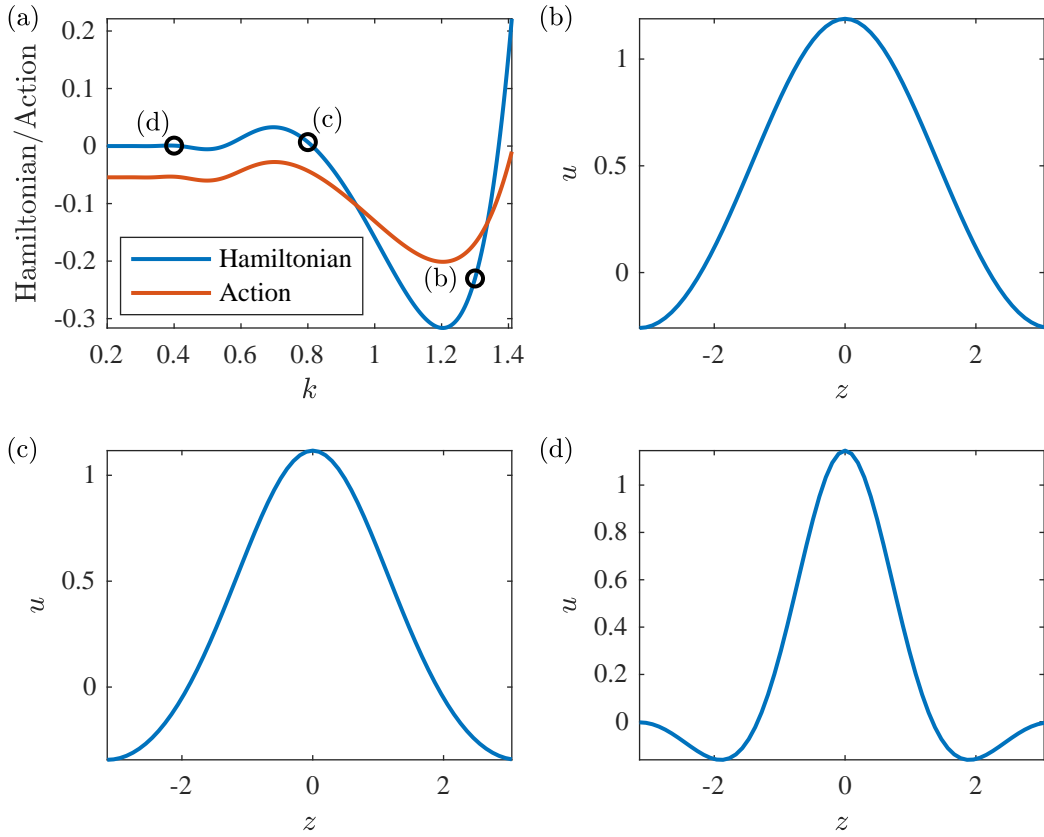


Figure 4: A family of periodic solutions of (2.4) with $\sigma = 1$. In panel (a) the Hamiltonian and Action are plotted as functions of k . Although H and A are qualitatively different, their critical points agree. Panels (b), (c) and (d) show plots of the periodic solutions $\hat{u}(z, k)$ as a function of z , with $-\pi < z < +\pi$, at three k -points along the curves.

$H = \frac{1}{4}$. The wavenumber is decreasing in Figure 4(a) with increasing amplitude.

The periodic solutions along the curves are hyperbolic, at least for small amplitude (near $k = \sqrt{2}, H = 1/4$). This follows since the constant states are saddle points: the characteristic equation (2.5) has two real roots and two purely imaginary.

Using the shooting algorithm, we will show that there exist heteroclinic connections between these two periodic orbits. For shooting we use the first-order form (1.4) which in this case is

$$(u_1)_x = u_2, \quad (u_2)_x = u_3, \quad (u_3)_x = u_4, \quad (u_4)_x = -\sigma u_3 - u_1 + u_1^3. \quad (2.6)$$

To find the connections, we will compute the stable and unstable foliations and track their intersection. The definition of a foliation starts with the asymptotic phase. Denote a vector-valued periodic solution of (2.6) by $\hat{\mathbf{u}}(z, k)$. A point in the stable manifold, \mathbf{u}_0 is said to have asymptotic phase θ if

$$\|\Phi(\mathbf{u}_0)(x) - \hat{\mathbf{u}}(z + \theta, k)\| \rightarrow 0 \quad \text{as } x \rightarrow +\infty, \quad (2.7)$$

where $\Phi(\mathbf{u}_0)$ is the flow of (2.6) with initial data \mathbf{u}_0 . Each asymptotic phase defines a leaf. A leaf is the union of all \mathbf{u}_0 with the same asymptotic phase. The union of these leaves over all asymptotic phases is the foliation. PALMER [39] proves the existence and uniqueness of the asymptotic phase, as well as the existence and smoothness of the foliation. An asymptotic phase on each of the periodic states at $\pm\infty$ is an essential part of the construction of the heteroclinic connection.

We follow the shooting strategy in KOON ET AL. [28] and KAHEMAN ET AL. [23] when computing a leaf of a foliation. It is initialized with a tangent vector of the periodic orbit using the linearization of (2.6) about the periodic orbit,

$$\frac{d}{dx} \begin{bmatrix} \delta u_1 \\ \delta u_2 \\ \delta u_3 \\ \delta u_4 \end{bmatrix} = \begin{bmatrix} 0 & 1 & 0 & 0 \\ 0 & 0 & 1 & 0 \\ 0 & 0 & 0 & 1 \\ -1 + 3\hat{u}^2 & 0 & -1 & 0 \end{bmatrix} \begin{bmatrix} \delta u_1 \\ \delta u_2 \\ \delta u_3 \\ \delta u_4 \end{bmatrix},$$

where δu_i represent small perturbations about the periodic orbit $\hat{u}^\pm(z, k)$. We compute the stable and unstable manifolds by integrating forward and backward in x , respectively, starting the integration by perturbing in the eigendirections corresponding to the stable or unstable Floquet multipliers. For the numerical computations carried out in this section, a typical perturbation amplitude is $\|\delta\mathbf{u}\| = 10^{-8}$. The foliation is constructed leaf by leaf by incrementing the phase along the periodic orbit.

To determine the heteroclinic connection, we compute the intersection of the invariant manifolds on an appropriate Poincaré section that is transverse to the foliations, as shown schematically in Figure 2. For the case at hand, a natural choice for the Poincaré section is $u_1 = 0$. The intersection points single out a leaf which is a candidate connection. The actual connection, and its asymptotic phase, is obtained by integrating from the Poincaré section back to the periodic orbit, along the chosen leaf.

In Figure 5, we present results for the case where $k = 1.38$. The geometry of the stable and unstable manifolds of the periodic orbits, the Poincaré section and corresponding heteroclinic connections are shown. They are plotted in the (u_1, u_2, u_3) space, and, in plates (d) and (f), as a function of x . Figure 5(a) shows the two periodic orbits in black, with centers at $u_1 = \pm 1$. The foliation of the unstable (stable) manifold of the periodic orbit near -1 is shown in red (blue).

Figure 5(b) shows the Poincaré section $u_1 = 0$ where the two manifolds meet as distorted ellipses and it is clear that they intersect in two points. These two points are then candidates for heteroclinic connections. In Figure 5(c)-(d), we include one of the heteroclinic connections which smoothly connects the two periodic orbits with the other connection shown in Figure 5(e)-(f). The connecting orbit is found by winding back leaves of the foliations to $\pm\infty$, starting with an intersection point. This calculation gives the asymptotic phases which we find to be $\pm\theta$, with $\theta \approx 1.36$ (in dimensionless units), giving the asymptotic behavior

$$\lim_{x \rightarrow \pm\infty} \|u(x) - \hat{u}^\pm(z \mp \theta, k)\| = 0. \quad (2.8)$$

Due to the $u \rightarrow -u$ symmetry and the fact that the action is sign-invariant, the actions of the two periodic orbits at infinity are equal.

2.2 Connecting asymmetric periodic orbits

It is possible to connect periodic orbits with different actions in multiple ways. One of which is to consider periodic solutions of equation (2.3) at $\pm\infty$ with different wavenumbers. Such a configuration has been studied by BANDARA

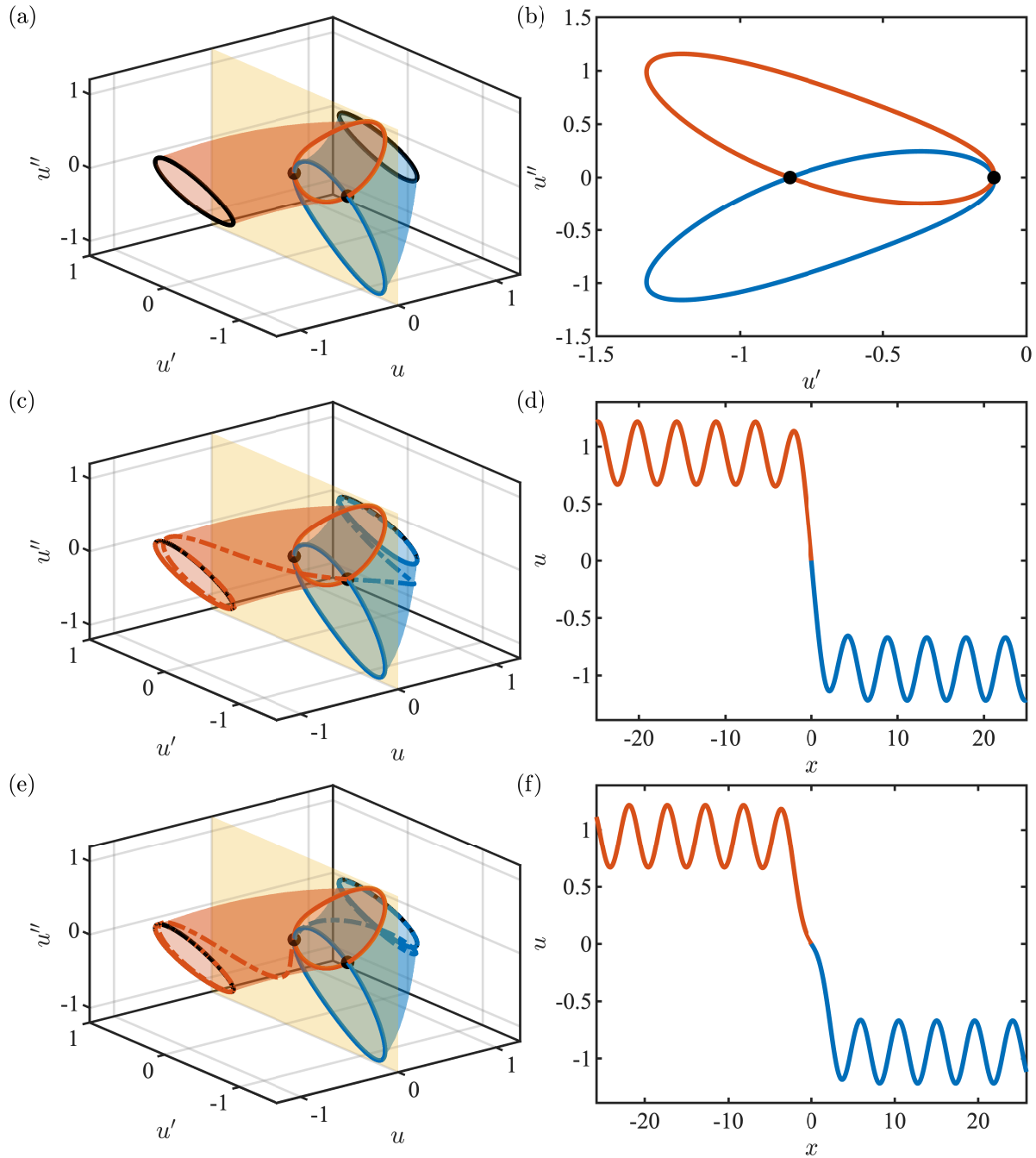


Figure 5: A plot of the stable and unstable foliations of the periodic orbits in (2.6). Panel (a) shows the stable and unstable manifolds (colored blue and red respectively) starting from the periodic orbits and ending on the (colored yellow) Poincaré section. Panel (b) shows a plot of the Poincaré section, with the two intersection points colored black. Panel (c) includes the manifolds along with the highlighted leaf which is the connection. That connection is shown as a function of x in panel (d). Panel (e) Shows a plot of the other heteroclinic connection on the manifolds and corresponding heteroclinic connection as a function of x is in (f)

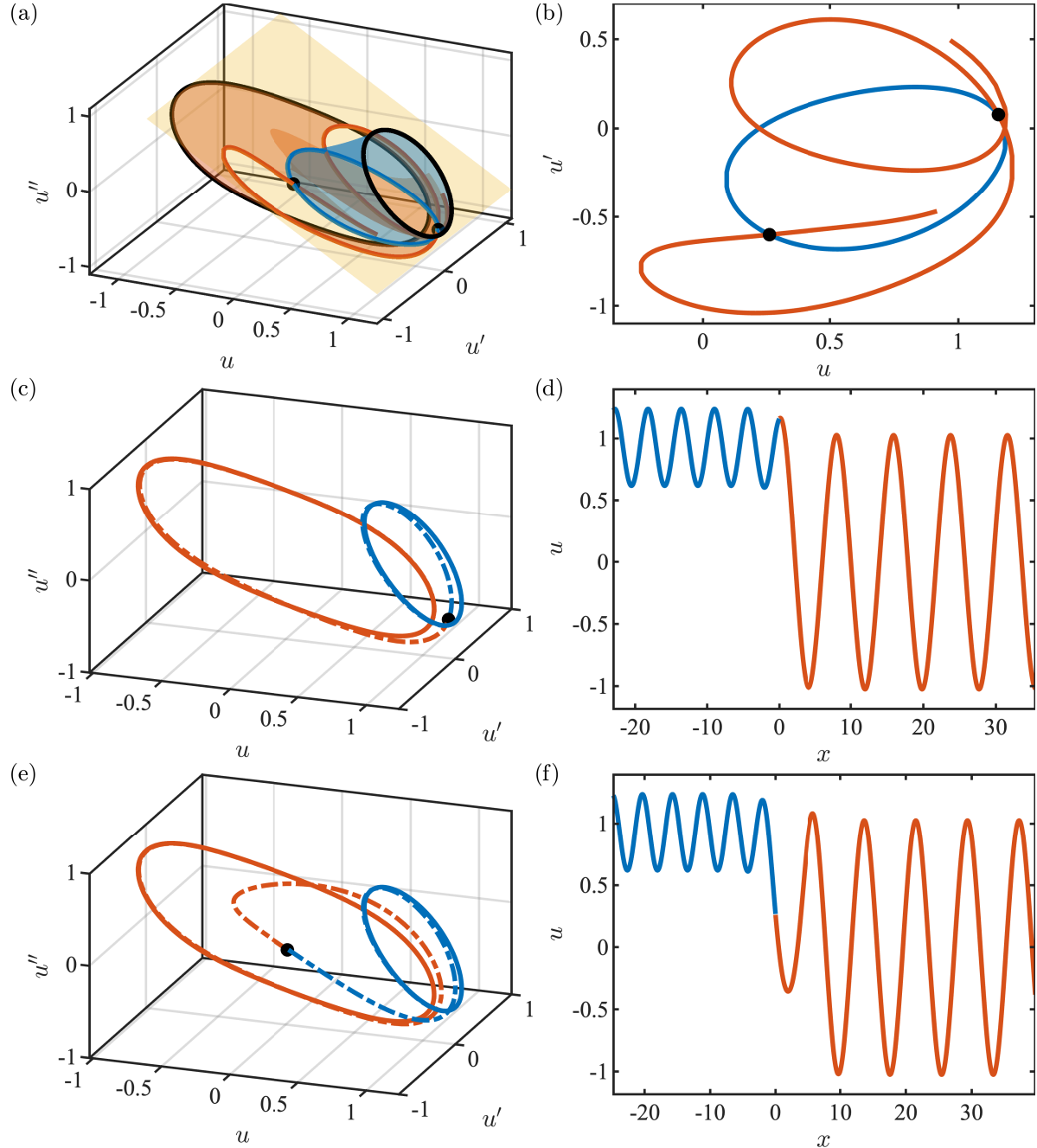


Figure 6: Panel (a) the stable manifold is shown in red and the unstable manifold is shown in blue with the Poincaré section at $u = 0$ shown in yellow. Panel (b) shows the stable and unstable manifolds on the Poincaré section with the two intersections identified with black dots. Panels (c) and (d) show one of the heteroclinic connections. Panels (e) and (f) show the other heteroclinic connection.

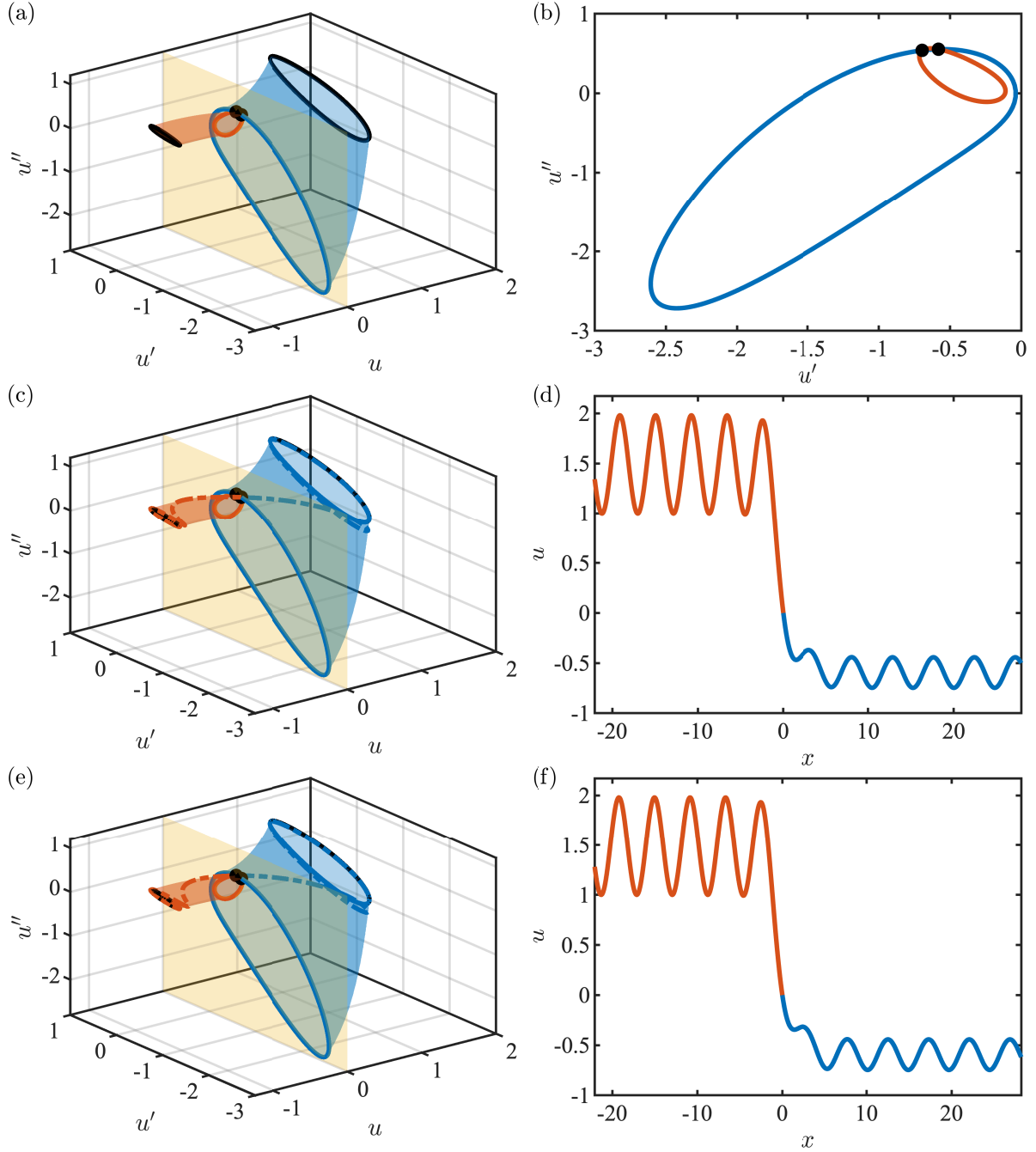


Figure 7: A plot of the stable and unstable manifolds and heteroclinic connections for the symmetry breaking case in (2.9). Panel (a) the stable manifold is shown in red and the unstable manifold is shown in blue with the Poincaré section at $u_1 = 0$ shown in yellow. Panel (b) shows the stable and unstable manifolds on the Poincaré section with the two intersections shown in black dots. Panels (c) and (d) show one of the heteroclinic connections and the corresponding manifolds. Panels (e) and (f) show the other heteroclinic connection and corresponding manifolds.

ET AL. [3]. We will recreate one of the cases in [3] by direct computations of the invariant manifolds of periodic solutions of equation (2.3) with $\sigma \approx 0.97$. The far-field hyperbolic periodic orbits have wavenumbers $k_+ \approx 1.365$ and $k_- \approx 0.799$. The wavenumbers are chosen so that the periodic orbits lie on the level set of the Hamiltonian $H = 0$. The corresponding actions of the periodic orbits are found to be $A_- \approx -0.18$ and $A_+ \approx -0.1268$, giving the jump $\Delta A = 0.0532$. Figure 6 shows the computed manifolds and the intersection with a surface of section,

$$1.744u_1 + 1.929u_3 = -0.807,$$

(the values of the coefficients are approximate). This Poincaré section is chosen as it effectively separates the two periodic orbits in the phase space. The stable and unstable manifolds of the periodic orbits are shown in red and blue, respectively. The surface of section is shown in yellow. The intersections of the stable and unstable manifolds in the Poincaré section are identified by black dots. Panels (c) and (d) show one of the heteroclinic connections, while panels (e) and (f) show the other heteroclinic connection. Note that the intersection of the stable manifold with the surface of section does not result in a closed loop. This result is attributed to the presence of an inverse-hyperbolic periodic orbit that lies between the two far-field periodic orbits. Indeed, a heteroclinic connection that is near this inverse-hyperbolic orbit is shown in Figure 6 (e) and (f).

2.3 Symmetry breaking

Another way to connect orbits with different actions is to include an explicit symmetry breaking term. The additional term considered here is the quadratic term u_1^2 that is added to the last equation in (2.6); that is, we investigate the equation

$$u_{xxxx} + u_{xx} + u + u^2 - u^3 = 0 \quad (2.9)$$

In Figure 7, we illustrate the geometry of the stable and unstable manifolds, the Poincaré section $u_1 = 0$, and the corresponding heteroclinic connections that link periodic orbits with wavenumbers $k_- = 1.503$ and $k_+ = 1.31$. These particular wavenumbers are selected to highlight the pronounced contrast in the amplitudes of the associated far-field periodic waves. Specifically, the periodic orbit on the left, corresponding to k_- , exhibits a significantly larger amplitude than the one on the right. This amplitude disparity is clearly reflected in the Poincaré section shown in Figure 7(b), where the orbit with smaller amplitude forms a more compact red loop, indicating a narrower projection in phase space. The action integrals associated with these far-field periodic orbits further quantify this difference: we compute $A_- = -0.638$ and $A_+ = -0.038$, respectively, giving the jump $\Delta A = 0.6$.

We now consider general properties of periodic orbits, introduce the codimension two normal form, and then study two examples that exhibit the singularity.

3 Properties of periodic orbits

We will use (1.1) for description of the theory, noting that it carries over to the Boussinesq system (1.24) and related models, with minor change. A periodic state of wavenumber k ,

$$\hat{u}(z, k), \quad \hat{u}(z + 2\pi, k) = \hat{u}(z, k), \quad z = kx, \quad (3.1)$$

satisfies

$$k^4 \hat{u}_{zzzz} + \sigma k^2 \hat{u}_{zz} + V'(\hat{u}) = 0. \quad (3.2)$$

The Hamiltonian function H in (1.3) is independent of the value of z , and can be used to parameterize solutions,

$$H = k^4 \hat{u}_z \hat{u}_{zzz} - \frac{1}{2} k^4 \hat{u}_{zz}^2 + \frac{1}{2} \sigma k^2 \hat{u}_z^2 + V(\hat{u}), \quad (3.3)$$

(using the same symbol H as in (1.3) to simplify notation).

Action is an invariant on solutions that is dual to the Hamiltonian function, in that it plays a similar role but is a relative invariant. Action is defined for an ensemble of solutions

$$u(x, s), \quad s \in (s_1, s_2), \quad (3.4)$$

where at this point (s_1, s_2) is just an open interval of real numbers. The ensemble can be thought of as parameterizing initial data, but this view is not essential. The ensemble is assumed to depend smoothly on s and satisfy (1.1) for each value of s ,

$$\frac{\partial^4}{\partial x^4}u(x, s) + \sigma \frac{\partial^2}{\partial x^2}u(x, s) + V'(u(x, s)) = 0, \quad \text{for each } s \in (s_1, s_2). \quad (3.5)$$

As shown in the introduction action is determined by a conservation law with the Lagrangian evaluated on the ensemble (1.17). This conservation law is confirmed by differentiating L in (1.2) with respect to s ,

$$\begin{aligned} L_s &= \partial_s (u_x u_{xxx} + \frac{1}{2}u_{xx}^2 + \frac{1}{2}\sigma u_x^2 - V(u)) \\ &= u_{xs} u_{xxx} + u_x u_{xxs} + u_{xx} u_{xss} + \sigma u_x u_{xs} - V'(u)u_s \\ &= (u_{xxx} u_s + u_x u_{xxs} + \sigma u_x u_s)_x - u_s (u_{xxxx} + \sigma u_{xx} + V'(u)), \end{aligned}$$

and noting that the second term on the right-hand side vanishes on solutions. The first term then gives the action

$$A(x, s) = u_{xxx} u_s + u_x u_{xxs} + \sigma u_x u_s. \quad (3.6)$$

The fact that A is an integral invariant follows by taking $s \in S^1$ and integrating the formula (1.17) over a period, giving

$$\frac{d}{dx} \oint_{S^1} (u_{xxx} u_s + u_x u_{xxs} + \sigma u_x u_s) \, ds = 0. \quad (3.7)$$

Figure 8 shows a schematic of action conservation. A closed curve of initial data has a value of action, and propagating this closed curve with the flow of the differential equation creates a cylinder, and the value of action is the same in each x -slice. When transformed to symplectic coordinates, this is an example of the Poincaré-Cartan theorem (see

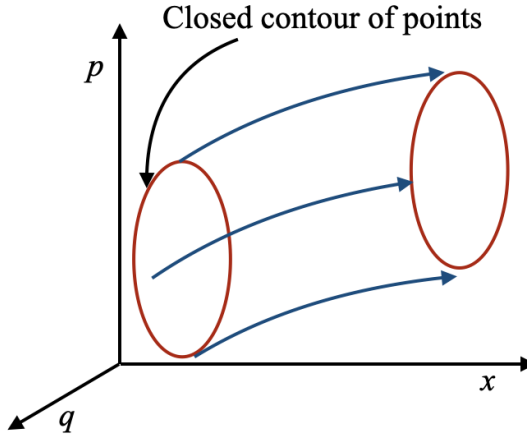


Figure 8: Illustration of the Poincaré-Cartan theorem, showing how a closed curve of initial data in the phase space carries a constant value of the action under the flow. (q, p) represent symplectic coordinates (see Appendix E).

Appendix E). It also explains why the value of the action integral is constant along the stable and unstable foliations, although the value is not defined on distinct leaves of a foliation. This property is in contrast to the Hamiltonian which is constant along each leaf.

A periodic orbit is a special case of an ensemble of points. We can evaluate A in (3.6) on a periodic orbit by taking $s = z$ and $x = z/k$, giving

$$A(k) = \frac{1}{2\pi} \int_0^{2\pi} (\sigma k \hat{u}_z^2 - 2k^3 \hat{u}_{zz}^2) dz, \quad (3.8)$$

(using the symbol A again to simplify notation). Since the value of action on a closed curve is an invariant (3.7), the value of $A(\hat{u})$ on the periodic orbits at $\pm\infty$ will be propagated on the stable and unstable foliations, when the curve in the integral (3.7) is taken to be transverse to the leaves. That is, each of the two cylinders in Figure 2 carries its own action invariant, determined by the value on the periodic orbit at infinity.

The formula (1.10) is proved as follows. The averaged Lagrangian is

$$\bar{L} = \frac{1}{2\pi} \int_0^{2\pi} (k^4 \hat{u}_z \hat{u}_{zzz} + \frac{1}{2} k^4 \hat{u}_{zz}^2 + \frac{1}{2} \sigma k^2 \hat{u}_z^2 - V(\hat{u})) dz. \quad (3.9)$$

Integrating by parts, and differentiating with respect to k gives $\bar{L}_k = A(k)$ for $A(k)$ in (3.8).

At points along the periodic orbits where $A_k \neq 0$ one pair of Floquet multipliers is at $+1$ and the other pair is either elliptic, hyperbolic, or coalesce at -1 . Figure 9 shows the two generic configurations. In all the results in this paper, the two periodic orbits are hyperbolic.



Figure 9: The two configurations of hyperbolic Floquet multipliers for periodic solutions of (1.1). The configuration on the left is called “inverse-hyperbolic” and on the right is “hyperbolic”.

The action values of the periodic orbits at $\pm\infty$ are not equal in general, and so there is a jump in the action when the two cylinders meet in the surface of section. This jump gives an intrinsic invariant of the connection

$$\Delta A := A(k^+) - A(k^-). \quad (3.10)$$

This property is new as far as we are aware. Examples with numerical values of this jump are in §2.1 and §2.3. On the other hand, the significance of this jump property is not apparent. The jump is zero when the two periodic orbits match: a homoclinic to the same periodic orbit, or when two periodic orbits are separated in phase space but are related by symmetry (an example is in §2.1). The action appears to be the same on each cylinder when the system is integrable, but we do not have a proof of this. The jump is intrinsic in the sense that it is invariant under symplectic change of coordinates; this follows by expressing the action in symplectic coordinates in which case the density is $\mathbf{p} \cdot d\mathbf{q}$ (see Appendix E).

It was pointed out in the introduction that action and the Hamiltonian function have critical points, $H_k = A_k = 0$, at the same value of k , along a branch of periodic orbits. We now prove this and give an illustration.

Lemma 3.1. *For the equation (1.1) with Hamiltonian H in (1.3) and action (3.8) evaluated on a family of periodic orbits with $k \neq 0$,*

$$H_k = k A_k. \quad (3.11)$$

Proof. First, since the value of H is independent of z , we have

$$H = \frac{1}{2\pi} \int_0^{2\pi} H dz = \frac{1}{2\pi} \int_0^{2\pi} \left(-\frac{3}{2} k^4 \hat{u}_{zz}^2 + \frac{1}{2} \sigma k^2 \hat{u}_z^2 + V(\hat{u}) \right) dz, \quad (3.12)$$

after integration by parts. Differentiate this expression with respect to k ,

$$H_k = \frac{1}{2\pi} \int_0^{2\pi} (-6k^3 \hat{u}_{zz}^2 - 3k^4 \hat{u}_{zz} \hat{u}_{zzk} + \sigma k \hat{u}_z^2 + \sigma k^2 \hat{u}_z \hat{u}_{zk} + V'(\hat{u}) \hat{u}_k) dz.$$

Rearrange, using the fact that \hat{u} is a solution

$$H_k = \frac{1}{2\pi} \int_0^{2\pi} \left(\sigma k \hat{u}_z^2 + 2\sigma k^2 \hat{u}_z \hat{u}_{zk} - 6k^3 \hat{u}_{zz}^2 - 4k^4 \hat{u}_{zz} \hat{u}_{zzk} + \left[k^4 \hat{u}_{zz} \hat{u}_{zzk} - \sigma k \hat{u}_z \hat{u}_{zk} + V'(\hat{u}) \hat{u}_k \right] \right) dz.$$

The term inside the square brackets vanishes on solutions (after integration by parts), leaving

$$H_k = \frac{1}{2\pi} \int_0^{2\pi} \left(\sigma k \hat{u}_z^2 + 2\sigma k^2 \hat{u}_z \hat{u}_{zk} - 6k^3 \hat{u}_{zz}^2 - 4k^4 \hat{u}_{zz} \hat{u}_{zzk} \right) dz.$$

Now differentiate $A(k)$ in (3.8),

$$A_k = \frac{1}{2\pi} \int_0^{2\pi} \left(\sigma \hat{u}_z^2 + 2\sigma k \hat{u}_z \hat{u}_{zk} - 6k^2 \hat{u}_{zz}^2 - 4k^3 \hat{u}_{zz} \hat{u}_{zzk} \right) dz.$$

Comparing the two proves the result. That is, when $k \neq 0$, we have $kA(k) = H(k)$. \square

Remark 3.2. *Although (3.11) was proved by direct calculation, it is in fact a consequence of the symplectic structure, and we will show that after the symplectic structure is introduced in Appendix E.*

An example of the lemma is shown in Figure 4, where actual calculations of periodic solutions of the cubic SH equation are used.

The equivalence of inflection points in (3.11) does not carry over to the second derivative since

$$H_{kk} = A_k + kA_{kk}.$$

However, when $A_k = 0$, then H_{kk} and A_{kk} are zero at the same value of k , when $k \neq 0$. This property will be useful in the normal form theory in §4.

Remark 3.3. *One of the main observations here is that parameterization of the periodic orbits via the Hamiltonian function (which is not uncommon) has the same key properties as parameterization by action (which is unheard of). Action is much easier to work with since it is always a quadratic function. Indeed, action in (3.8) is a linear combination of the (square of the) $H^1(S^1)$ and $H^2(S^1)$ Sobolev norms.*

3.1 Action and algebraic multiplicity

The linearization about a periodic state brings in Floquet theory, but it is a little more interesting in that the spectral problem is nonlinear in the parameter. The most interesting feature is how action feeds into the Jordan chain theory.

Let $u = \hat{u} + \tilde{v}(z, x)$, substitute into (1.1), and linearize about \hat{u} ,

$$\left(\frac{\partial}{\partial x} + k \frac{\partial}{\partial z} \right)^4 \tilde{v} + \sigma \left(\frac{\partial}{\partial x} + k \frac{\partial}{\partial z} \right)^2 \tilde{v} + V'(\hat{u}) \tilde{v} = 0. \quad (3.13)$$

Introduce a spectral ansatz in x , $\tilde{v}(z, x) = e^{\lambda x} v(z, \lambda)$, giving the nonlinear in the parameter spectral problem

$$\mathbf{L}(\lambda)v := \left(\lambda + k \frac{\partial}{\partial z} \right)^4 v + \sigma \left(\lambda + k \frac{\partial}{\partial z} \right)^2 v + V''(\hat{u})v. \quad (3.14)$$

The tangent vector to the solution is an eigenvector with eigenvalue zero,

$$\mathbf{L}(0)\xi_1 = 0, \quad \text{with} \quad \xi_1 = \hat{u}_z. \quad (3.15)$$

We assume the the geometric multiplicity is one. We define algebraic multiplicity for a nonlinear in the parameter eigenvalue problem following MAGNUS [34], RABIER [42], and LÓPEZ-GÓMEZ & MORA-CORRAL [32]. We have the following result from the above references, stated for the case needed here (geometric multiplicity one and algebraic multiplicity four).

Proposition 3.4. [32, 34, 42] Suppose an eigenvalue λ_* of $\mathbf{L}(\lambda)$ has geometric multiplicity one and algebraic multiplicity four. Then there exists a Jordan chain ξ_1, \dots, ξ_4 , with ξ_1 the geometric eigenvector satisfying

$$\mathbf{L}(\lambda_*)\xi_1 = 0,$$

and three generalized eigenvectors satisfying

$$\begin{aligned}\mathbf{L}(\lambda_*)\xi_2 &= -\mathbf{L}'(\lambda_*)\xi_1 \\ \mathbf{L}(\lambda_*)\xi_3 &= -\mathbf{L}'(\lambda_*)\xi_2 - \frac{1}{2}\mathbf{L}''(\lambda_*)\xi_1 \\ \mathbf{L}(\lambda_*)\xi_4 &= -\mathbf{L}'(\lambda_*)\xi_3 - \frac{1}{2}\mathbf{L}''(\lambda_*)\xi_2 - \frac{1}{3!}\mathbf{L}'''(\lambda_*)\xi_1.\end{aligned}$$

Moreover, when $\mathbf{L}(\lambda_*)$ is self-adjoint, the chain ends at four when

$$\left\langle \left\langle \xi_1(z), -\mathbf{L}'(\lambda_*)\xi_4 - \frac{1}{2}\mathbf{L}''(\lambda_*)\xi_3 - \frac{1}{3!}\mathbf{L}'''(\lambda_*)\xi_2 - \frac{1}{4!}\mathbf{L}''''(\lambda_*)\xi_1 \right\rangle \right\rangle \neq 0, \quad (3.16)$$

where the inner product is for periodic scalar-valued functions,

$$\langle\langle a, b \rangle\rangle := \frac{1}{2\pi} \int_0^{2\pi} a(z)b(z) dz. \quad (3.17)$$

Applying this result to (3.14) with $\lambda_* = 0$ and the geometric eigenvector ξ_1 satisfying (3.15), the chain $(\xi_1, \xi_2, \xi_3, \xi_4)$ is defined by

$$\begin{aligned}\mathbf{L}(0)\xi_1 &= 0 \\ \mathbf{L}(0)\xi_2 &= -\left(4k^3 \frac{\partial^3}{\partial z^3} \xi_1 + 2\sigma k \frac{\partial}{\partial z} \xi_1\right) \\ \mathbf{L}(0)\xi_3 &= -\left(4k^3 \frac{\partial^3}{\partial z^3} \xi_2 + 2\sigma k \frac{\partial}{\partial z} \xi_2\right) - 6k^2 \frac{\partial^2}{\partial z^2} \xi_1 - \sigma \xi_1 \\ \mathbf{L}(0)\xi_4 &= -\left(4k^3 \frac{\partial^3}{\partial z^3} \xi_3 + 2\sigma k \frac{\partial}{\partial z} \xi_3\right) - \left(6k^2 \frac{\partial^2}{\partial z^2} \xi_2 + \sigma \xi_2\right) - 4k \frac{\partial}{\partial z} \xi_1.\end{aligned} \quad (3.18)$$

For the spectral problem (3.14), the algebraic multiplicity is automatically two, since the ξ_2 equation is solvable,

$$\left\langle \left\langle \xi_1, -\left(4k^3 \frac{\partial^3}{\partial z^3} \xi_1 + 2\sigma k \frac{\partial}{\partial z} \xi_1\right) \right\rangle \right\rangle = 0.$$

That this expression is zero can be verified using integration by parts. There is also an explicit expression for ξ_2 , which is obtained by differentiating the governing equation for \hat{u} in (3.2) with respect to k ,

$$k^4(\hat{u}_k)_{zzzz} + \sigma k^2(\hat{u}_k)_{zz} + V''(\hat{u})\hat{u}_k + 4k^3\hat{u}_{zzzz} + 2\sigma k\hat{u}_{zz} = 0. \quad (3.19)$$

This is the equation for ξ_2 , giving

$$\xi_2 = \hat{u}_k + C\hat{u}_z,$$

where C is an arbitrary constant. The most interesting result is the condition for algebraic multiplicity three, which brings in the action.

Proposition 3.5. Suppose the above spectral problem has $\lambda = 0$ as an eigenvalue of geometric multiplicity one. The algebraic multiplicity is automatically two. The algebraic multiplicity is three if and only if $A_k = 0$. Moreover when it is three it is automatically four.

Proof. Algebraic multiplicity two is proved above. Algebraic multiplicity three follows if the ξ_3 equation is solvable; that is

$$\left\langle \left\langle \xi_1, -\left(4k^3 \frac{\partial^3}{\partial z^3} \xi_2 + 2\sigma k \frac{\partial}{\partial z} \xi_2\right) - 6k^2 \frac{\partial^2}{\partial z^2} \xi_1 - \sigma \xi_1 \right\rangle \right\rangle = 0.$$

Integrating by parts and using $\xi_1 = \hat{u}_z$ and $\xi_2 = \hat{u}_k$, gives

$$\left\langle \left\langle \hat{u}_z, - \left(4k^3 \frac{\partial^3}{\partial z^3} \hat{u}_k + 2\sigma k \frac{\partial}{\partial z} \hat{u}_k \right) - 6k^2 \frac{\partial^2}{\partial z^2} \hat{u}_z - \sigma \hat{u}_z \right\rangle \right\rangle. \quad (3.20)$$

Noting that

$$A_k = \frac{1}{2\pi} \int_0^{2\pi} (\sigma \hat{u}_z^2 + 2\sigma k \hat{u}_z \hat{u}_{zk} - 6k^2 \hat{u}_{zz}^2 - 4k^3 \hat{u}_{zz} \hat{u}_{zzk}) dz,$$

for $A(k)$ defined in (3.8) shows that the integral in (3.20) is $-A_k$. This proves that algebraic multiplicity three is in one-to-one correspondence with $A_k = 0$. That the algebraic multiplicity is automatically four follows from solvability of the ξ_4 equation, which can be verified by direct calculation. That completes the proof. \square

Although we have used the nonlinear in the parameter theory, the above Jordan chain and multiplicity results are a consequence of the underpinning symplectic structure and comments on this are in Appendix E.

The algebraic multiplicity of the above eigenvalue problem will terminate at four if the equation for ξ_5 is not solvable,

$$\mathbf{L}(0)\xi_5 = - \left(4k^3 \frac{\partial^3}{\partial z^3} \xi_4 + 2\sigma k \frac{\partial}{\partial z} \xi_4 \right) - \left(6k^2 \frac{\partial^2}{\partial z^2} \xi_3 + \sigma \xi_3 \right) - 4k \frac{\partial}{\partial z} \xi_2 - \xi_1. \quad (3.21)$$

Checking solvability,

$$\left\langle \left\langle \xi_1, \left(4k^3 \frac{\partial^3}{\partial z^3} \xi_4 + 2\sigma k \frac{\partial}{\partial z} \xi_4 \right) + \left(6k^2 \frac{\partial^2}{\partial z^2} \xi_3 + \sigma \xi_3 \right) + 4k \frac{\partial}{\partial z} \xi_2 + \xi_1 \right\rangle \right\rangle \neq 0.$$

Integrate by parts and use periodicity

$$-4k^3 \left\langle \left\langle \frac{\partial^3}{\partial z^3} \xi_1, \xi_4 \right\rangle \right\rangle - 2\sigma k \left\langle \left\langle \frac{\partial}{\partial z} \xi_1, \xi_4 \right\rangle \right\rangle + 6k^2 \left\langle \left\langle \frac{\partial^2}{\partial z^2} \xi_1, \xi_3 \right\rangle \right\rangle + \sigma \left\langle \left\langle \xi_1, \xi_3 \right\rangle \right\rangle - 4k \left\langle \left\langle \frac{\partial}{\partial z} \xi_1, \xi_2 \right\rangle \right\rangle + \left\langle \left\langle \xi_1, \xi_1 \right\rangle \right\rangle \neq 0.$$

Now, note that $\xi_1 = \hat{u}$ and substitute

$$-4k^3 \left\langle \left\langle \hat{u}_{zzzz}, \xi_4 \right\rangle \right\rangle - 2\sigma k \left\langle \left\langle \hat{u}_{zz}, \xi_4 \right\rangle \right\rangle + 6k^2 \left\langle \left\langle \hat{u}_{zzzz}, \xi_3 \right\rangle \right\rangle + \sigma \left\langle \left\langle \hat{u}_z, \xi_3 \right\rangle \right\rangle - 4k \left\langle \left\langle \hat{u}_{zz}, \xi_2 \right\rangle \right\rangle + \left\langle \left\langle \hat{u}_z, \hat{u}_z \right\rangle \right\rangle \neq 0. \quad (3.22)$$

This condition should be satisfied for termination of the chain at four. We will find that this expression is precisely the coefficient \mathcal{K} in the normal form in (1.15) and (7.1).

Remark 3.6. *It is well known in the pattern formation literature and in the celestial mechanics literature, for example, that $H_k = 0$ signals a turning point in a branch of periodic solutions. What is surprising here is that the above direct proof of this is in terms of $A_k = 0$, with the association with $H_k = 0$ following indirectly from (3.11).*

4 Nonlinear normal form theory

In this section, we discuss the form and features of the nonlinear normal form that describes the wavenumber modulation near the codimension two point, $A_k = A_{kk} = 0$, using phase modulation [21]. We then impose the symplectic structure on the phase modulation to prove that the key coefficient in the normal form is related to the action.

The emergence of the normal form starts with the ansatz

$$u(x) = \hat{u}(z + \phi, k_0 + \varepsilon q) + \varepsilon^2 w(z + \phi, X, \varepsilon), \quad (4.1)$$

where k_0 is the wavenumber of the unperturbed wave and

$$X = \varepsilon x, \quad q = \phi_X, \quad \varepsilon^2 w = \varepsilon^2 w_2 + \varepsilon^3 w_3 + \varepsilon^4 w_4 + \dots \quad (4.2)$$

The ansatz (4.1) is substituted into (1.1), everything is expanded in Taylor series in ε , and solved order by order. The full details of this procedure can be found in Appendix B, but we note here the central role of action. The conditions $A_k(k_0) = 0$ and $A_{kk}(k_0) = 0$ arise as solvability conditions within the analysis for the q_X and qq_X terms, in the normal form, respectively. The former of these is the primary singularity in the modulation approach, and results in the emergence of a third order derivative in the normal form. The second of these brings in the cubic nonlinearity as a natural consequence, taking the role of the dominant nonlinearity in the normal form. As confirmed by a direct asymptotic analysis in Appendix B, we obtain the normal form at the critical point:

$$\frac{1}{2}A_{kkk}(k_0)q^2q_X + \mathcal{K}q_{XXX} = 0. \quad (4.3)$$

The coefficient \mathcal{K} of the spatial derivative can be characterized various ways. It emerges as a solvability condition in the Jordan chain theory (e.g. Equation (3.22)), and can also be characterized using symplectic Jordan chain theory. Here we will relate it to the Bloch spectrum of the basic wavetrain $\mu(\nu; k)$ via

$$\mathcal{K} = \frac{1}{24}\mu'''(0; k_0) \quad (4.4)$$

where primes denote derivatives with respect to ν . This formula is proved in Appendix D. The connection between dispersion and the Bloch exponent was first identified in dissipative pattern forming systems [17] and later generalized to Hamiltonian systems, and related to Krein signature, in [43]. The result is a normal form that can be constructed entirely using properties of the original wave - its action and its Bloch spectrum - which can be computed independently of the asymptotic analysis.

The analysis of this paper is interested in behavior in the vicinity of this codimension 2 point, where the heteroclinic connections develop further, and thus we must introduce an unfolding of the codimension 2 point. Formally, the resulting asymptotic balance requires that

$$A_k(k_0) = \mathcal{O}(\varepsilon^2), \quad A_{kk}(k_0) = \mathcal{O}(\varepsilon),$$

and in the sequel we will assume the asymptotic constants associated with these orderings is α and β respectively. Examples of these asymptotic constants and how they can be obtained is given in §4.1. In such cases, the generic unfolding of the codimension 2 point is as follows:

$$\frac{1}{2}A_{kkk}(k_0)q^2q_X + \alpha q_X + \beta qq_X + \mathcal{K}q_{XXX} = 0. \quad (4.5)$$

The details of the derivation of (4.3) are given in Appendix B. It is the unfolded version (4.5) that we will explore in this paper, as it has explicit heteroclinic connections, noting that the true codimension 2 point follows by setting $\alpha = \beta = 0$.

4.1 Heteroclinic connections via the normal form

We now explore (4.5) to determine the criterion for heteroclinic connections and their mathematical form. We start by integrating (4.5) once, resulting in the ODE

$$\mathcal{K}q_{XX} + \alpha q + \frac{1}{2}\beta q^2 + sq^3 + I = 0, \quad s = \frac{1}{6}A_{kkk} \quad (4.6)$$

where I is the a constant of integration. We can see that I plays the role of the action of this orbit evaluated on the original unperturbed wave. This can best be seen comparing the Taylor series of the action,

$$A(k) \approx A(k_0) + A_k(k_0)(k - k_0) + \frac{1}{2}A_{kk}(k_0)(k - k_0)^2 + \frac{1}{6}A_{kkk}(k_0)(k - k_0)^3$$

to the polynomial terms in (4.6), recalling the definitions of α and β , and noting that $k - k_0 \approx \varepsilon q$. It is useful to our discussion to notice that (4.6) is of the form of a kinetic-potential Hamiltonian system, with Hamiltonian

$$H_{NF}(q, q_X) = \frac{1}{2}\mathcal{K}q_X^2 + Iq + \frac{1}{2}\alpha q^2 + \frac{1}{6}\beta q^3 + \frac{s}{4}q^4 \equiv \frac{1}{2}\mathcal{K}q_X^2 + \mathcal{H}(q),$$

where crucially we note the potential function \mathcal{H} is quartic. The remainder of our analysis will be to determine the conditions on this quartic potential that permit heteroclinic connections in the wavenumber q and thus a PtoP connection of the original underlying wave.

Constant solutions of the normal form (4.6) correspond to periodic orbits of (1.1) and are those with fixed action, satisfying

$$I + \alpha q + \frac{1}{2}\beta q^2 + sq^3 = 0. \quad (4.7)$$

This is to say that they minimize the potential function \mathcal{H} , as the above polynomial corresponds to the condition $\mathcal{H}'(q) = 0$. Two solutions of this equation are called conjugate periodic orbits if they both satisfy (4.7) for the same value of I and H_{NF} .

Remark 4.1. *As equilibria of the normal form conjugate orbits have the same action and Hamiltonian, since the normal form is integrable. However, when lifted to the phase space, the representative periodic orbits will not, in most cases, have the same action, although they will have the same value of the Hamiltonian.*

Another property of conjugate periodic orbits is that they share the same potential energy $\mathcal{H}(q)$. Thus, our criterion for conjugate states is entirely determined by the shape of the potential energy - it must possess two extrema that occur at the same energy level. As such, our condition for conjugate states reduces to requiring that $\mathcal{H}(q)$ is of the form

$$\mathcal{H}(q) = \frac{s}{4}(q - Q_1)^2(q - Q_2)^2$$

for two real numbers $Q_1 \neq Q_2$. We now seek to find the general form of the conjugate states in terms of the coefficients of the normal form. Denote the two solutions of this problem by Q_1 and Q_2 with $Q_1 \neq Q_2$. By definition of these being conjugate states, we must have the following two conditions for minimizing the potential energy,

$$\begin{aligned} 0 &= I + \alpha Q_1 + \frac{1}{2}\beta Q_1^2 + sQ_1^3 \\ 0 &= I + \alpha Q_2 + \frac{1}{2}\beta Q_2^2 + sQ_2^3, \end{aligned} \quad (4.8)$$

and a third condition that they possess the same potential energy value,

$$IQ_1 + \frac{1}{2}\alpha Q_1^2 + \frac{1}{6}\beta Q_1^3 + \frac{s}{4}Q_1^4 = \mathcal{H} = IQ_2 + \frac{1}{2}\alpha Q_2^2 + \frac{1}{6}\beta Q_2^3 + \frac{s}{4}Q_2^4. \quad (4.9)$$

The aim now is to solve the three equations (4.8) and (4.9) for the three unknown Q_1, Q_2, I . Surprisingly, there is an explicit exact solution. The details are lengthy and will be skipped. The result is

$$Q_1 = -\frac{\beta}{6s} \pm \frac{1}{s}\sqrt{D} \quad \text{and} \quad Q_2 = -Q_1 - \frac{\beta}{3s}, \quad D = \frac{1}{12}\beta^2 - s\alpha, \quad (4.10)$$

where the sign in the first term is chosen so that $Q_1 < Q_2$. Thus, we find a necessary condition for the heteroclinic connections to exist by imposing our roots must be real, requiring that

$$\frac{1}{12}\beta^2 - s\alpha \geq 0 \quad \Rightarrow \quad A_{kk}(k_0)^2 \geq 2A_k(k_0)A_{kkk}(k_0). \quad (4.11)$$

Back substitute a solution to find expressions for the action I and \mathcal{H} ,

$$I = \frac{\beta}{108s^2} (18s\alpha - \beta^2), \quad \mathcal{H} = -\frac{(18s\alpha - \beta^2)^2}{1296s^3} = -\frac{9s}{\beta^2}I^2. \quad (4.12)$$

Hence for any $(\alpha, \beta) \in \mathbb{R}^2$ with $\alpha, \beta = o(\varepsilon^{-1})$, these formulas give the values of I and \mathcal{H} at which conjugate periodic orbits Q_1 and Q_2 in (4.10) exist.

This gives the existence of conjugate periodic orbits. The next necessary condition for a heteroclinic connection is that both conjugate periodic orbits be hyperbolic. Hyperbolicity is determined by linearizing (4.6) about either constant state, denoted by Q_0 ,

$$\mathcal{K}\delta Q_{XX} + (\alpha + \beta Q_0 + 3sQ_0^2)\delta Q = 0. \quad (4.13)$$

Hence a basic state is hyperbolic when

$$\text{sign}(\mathcal{K}\mathcal{H}''(Q_0)) < 0.$$

Substitution of either Q_1 or Q_2 into this condition reveals the two solutions are hyperbolic when

$$\frac{\mathcal{K}}{s} \left(\frac{1}{12} \beta^2 - s\alpha \right) < 0.$$

As the bracketed term is assumed positive for the existence of the conjugate states, we therefore have the condition for hyperbolicity as

$$\text{sign}(\mathcal{K}s) \equiv \text{sign}(\mathcal{K}A_{kkk}(k_0)) < 0,$$

i.e. that the underlying stationary modified KdV is defocussing, in line with previous studies on the stability of solutions within equations of this type [14, 24, 18]. This observation, as well as the condition for existence, are summarized as follows.

Let $\hat{u}(k_0 x + \theta_0) \equiv \hat{u}(z)$ be a periodic solution of (1.1). Suppose a local wavenumber perturbation k is introduced such that $|k - k_0| \ll 1$. Then, provided that

$$A_k(k_0) = \mathcal{O}(|k - k_0|^2), \quad A_{kk}(k_0) = \mathcal{O}(|k - k_0|),$$

a hyperbolic pair of conjugate states representing a heteroclinic connection between two periodic states emerges from the point $A_k(k_0) = A_{kk}(k_0) = 0$ provided that

$$A_{kk}(k_0)^2 \geq 2A_k(k_0)A_{kkk}(k_0) \quad \text{and} \quad \text{sign}(\mu'''(0; k_0)A_{kkk}(k_0)) < 0,$$

where $\mu(\nu; k_0)$ is the Bloch spectrum of the wavetrain $\hat{u}(z)$.

To finish our discussion here, we provide the explicit form of the heteroclinic connection between the two wavetrains as prescribed by the normal form (4.6). This can most readily be obtained by multiplying this equation by q_X and integrating once with respect to X and prescribing the conditions for a repeated double root of the resulting quartic polynomial (requiring (4.11) to hold) and assuming $\mathcal{K}s < 0$. In such a case, we end up with the first order ODE

$$q_X = \pm \sqrt{-\frac{s}{4\mathcal{K}}} (q - Q_1)(Q_2 - q), \quad Q_1 < q < Q_2.$$

This has a pair of tanh solutions, one for each sign of the right-hand side:

$$q(X) = \frac{(Q_1 + Q_2)}{2} \pm \frac{(Q_2 - Q_1)}{2} \tanh(\delta X), \quad \delta = \sqrt{\left| \frac{s}{4\mathcal{K}} \right|} \frac{(Q_2 - Q_1)}{2\sqrt{2}},$$

This gives a prototypical heteroclinic connection between two asymptotic wavenumbers $k_0 + \varepsilon Q_1$ and $k_0 + \varepsilon Q_2$. The strength of the connection (i.e. its amplitude) is precisely the difference between the two roots. The above form also highlights that the strength of the connection, the strength of the cubic term in (4.6) and the Bloch spectrum all control the width of the heteroclinic connection. The resulting perturbed wave phase is

$$\phi(X) = \int Q(Y) dY = \frac{(Q_1 + Q_2)}{2} X \pm \frac{Q_2 - Q_1}{2\delta} \ln(\cosh(\delta X)) + \phi_0 \equiv \phi_0 + \varepsilon \frac{Q_1 + Q_2}{2} x + \frac{Q_2 - Q_1}{2\delta} \ln(\cosh(\varepsilon\delta x)).$$

The phase is unbounded as $x \rightarrow \pm\infty$, but it is asymptotically consistent and of lower order than the original wave phase:

$$\lim_{\varepsilon \rightarrow 0} \left| \frac{\phi}{z} \right| < \lim_{\varepsilon \rightarrow 0} \frac{\varepsilon Q_2}{2k_0} \rightarrow 0$$

Finally, we note that this approximation and explicit solution do not give us the selected asymptotic phases of the periodic orbits, and geometrically corresponds to the special case where the two cylinders shown in Figure 2 are identical and intersect perfectly such that the two circles on the Poincaré section overlap, due to integrability of the normal form. In order to capture the splitting of the circles on the Poincaré section asymptotically, we would need to go to higher order and possibly beyond all orders and we leave this for future work.

5 The SH357 equation

The next two sections are based on the SH357 equation introduced by KNOBLOCH ET AL. [26]. It is of the form (1.1) but with a higher order nonlinearity

$$u_{xxxx} + 2u_{xx} + (1 - \mu)u + au^3 - bu^5 + u^7 = 0, \quad (5.1)$$

replacing λ in [26] by μ and noting that $\sigma = 2$. Our main new result is the discovery of two codimension 2 points in this system, one of which has the right signs and produces an organizing center for a branch of heteroclinic connections. Before presenting the results, we review some of the relevant results in [26]. Their strategy for computing families of periodic solutions, as a precursor to connecting them, is very different from this paper in an interesting way. They work from a bifurcation perspective, with bifurcation parameter μ , whereas we work from a symplectic perspective, with emphasis on the action, Hamiltonian, and wavenumber spaces.

We have re-calculated some of their results for validation. Figure 10 shows our recalculation of Figure 1, Panel (a) in [26]. It shows a branch of periodic orbits plotted in the μ versus $\|u\|$ plane on the left, and the Hamiltonian versus μ on the right. Our results match [26] to graphical accuracy. An interesting property of the left diagram is that the turning points correspond to a change in temporal stability and give no information about spatial Floquet multipliers. This latter observation follows by noting that periodic solutions are critical points of

$$\mathcal{E}(u, \mu) = \int_{\Omega} \left[\frac{1}{2} u_{xx}^2 + uu_{xx} - \frac{1}{2}(\mu - 1)u^2 - F(u) \right] dx \quad (5.2)$$

with $F'(u) = -au^3 + bu^5 - u^7$, and $\Omega \subset \mathbb{R}$ (and $\Omega = S^1$ in the periodic case). A key functional is

$$-\mathcal{E}_{\mu} = \frac{1}{2} \|u\|^2.$$

MADDOCKS [33] proves, for general functionals of the form (5.2), that turning points in the $(\lambda, -\mathcal{E}_{\mu})$ plane correspond to changes of (temporal) stability. This agrees with Figure 10 (and Figure 1(a) in [26]), since $\|u\| = \sqrt{-2\mathcal{E}_{\mu}}$. Note also that the plots of H versus μ are dramatically different from H or A versus k . In the (H, μ) -plane, turning points appear as cusps. This feature is predicted by gradient μ -based bifurcation theory (compare with Figure 3 of THOMPSON [51]). We cannot just re-plot the (H, μ) plots in the (H, k) plane because the wavenumber is fixed in

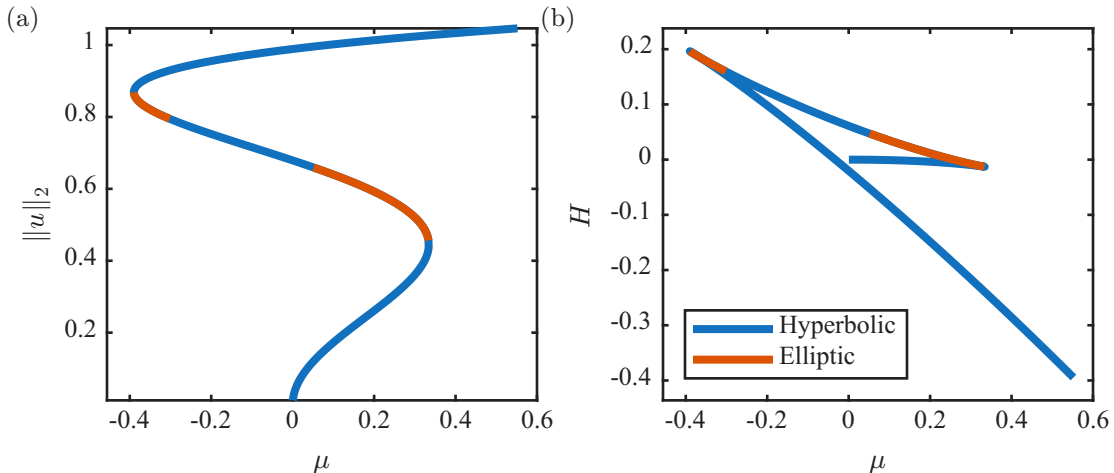


Figure 10: Our re-calculation of Figure 1, Panel (a), from KNOBLOCH ET AL. [26]. Turning points on the left panel correspond to changes in temporal stability. We have added in our calculation of spatial Floquet multipliers, with blue indicating hyperbolic Floquet multipliers.

the (H, μ) plane. We will approach the problem afresh using our strategy of plotting H (or A) versus wavenumber

as this gives *bifurcation of spatial Floquet multipliers at turning points*. This strategy will be all the more important when we search for codimension 2 points as they appear naturally in the (A, k) and (H, k) space and do not appear in μ -based planes.

With three parameters and strong nonlinearity, the SH357 equation provides an excellent test case for finding codimension two points.

5.1 Finding and continuing codimension two points

In this subsection, we present a numerical algorithm for computing the codimension two points, $A_k = A_{kk} = 0$, in a field of periodic orbits. The algorithm is more general (and is applied to the ac-Boussinesq in §6), but will be developed in the context of the SH357 equation. Step one is to identify a codimension 1 singularity; that is, a line or surface $A_k(k, \cdot) = 0$, where the dot represents other parameters. Step two is to continue this singularity in a two-parameter space until a codimension 2 point is hit. The third step is to calculate heteroclinic connections in the unfolding of the singularity.

We will use $\hat{u}(z, k, \mu, a, b)$ to denote a multiparameter field of 2π -periodic orbits (sometimes suppressing the parameters for brevity). In step one, the parameters μ and a are fixed, and then we work in a two-parameter family of periodic orbits parameterized by k and b . We compute a codimension 1 curve in the (k, b) space, parameterized by s , in some interval $s_1 < s < s_2$. The parameterized curve $(k(s), b(s))$ is defined by

$$\partial_k A(k(s), b(s)) = 0 \quad (\text{with } a, \mu \text{ fixed}). \quad (5.3)$$

Figure 11 shows various perspectives on the set defined by (5.3) in the case $\mu = 0.3$ and $a = 1.5$.

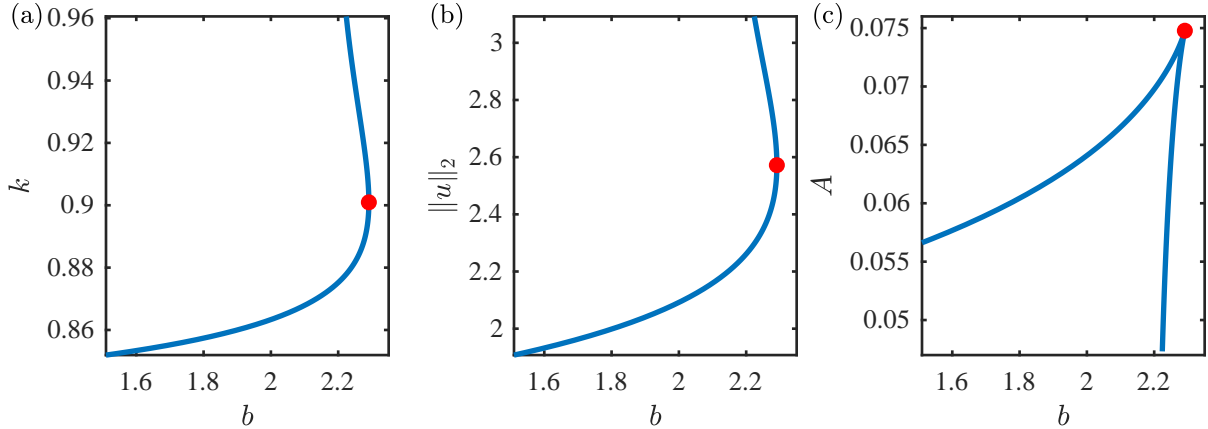


Figure 11: (a) Plot of the curve $(k(s), b(s))$ generated by solving (5.3) for the family of periodic orbits of (5.1) with $\mu = 0.3$ and $a = 1.5$. (b) A plot of the L^2 norm of the solution along the same curve as (a). (c) A plot of the action, A , along the same solution curve

In principle, the codimension two point can be identified by computing $\partial_k^2 A(k, b)$ along the codimension one curves looking for points where it changes sign. However, we will show that there is an easier way. The relation of the geometry of the (k, b) -curve to the action derivatives is summarized in the following.

Lemma 5.1. *Suppose that the curve $(k(s), b(s))$ satisfying $A_k(k(s), b(s)) = 0$ is smooth (at least differentiable), for $s_1 < s < s_2$. For some $s^* \in (s_1, s_2)$, suppose that $b'(s^*) = 0$, $k'(s^*) \neq 0$, and $A_{kb}(k(s^*), b(s^*)) \neq 0$, then $(k(s^*), b(s^*))$ corresponds to a codimension two point:*

$$A_k(k(s), (s)) = A_{kk}(k(s), b(s)) = 0 \quad \Leftrightarrow \quad k'(s) \neq 0 \text{ and } b'(s) = 0, \quad \text{for some } s^* \in (s_1, s_2). \quad (5.4)$$

Proof. Since the curve is smooth, the function

$$f(s) := A_k(k(s), b(s)),$$

is zero for each s and differentiable. Therefore

$$0 = f'(s) = A_{kk}(k(s), b(s))k'(s) + A_{kb}(k(s), b(s))b'(s).$$

The claim (5.4) is then immediate. \square

In Fig. 11, the codimension two point found with this Lemma is identified with a red dot. It is associated with a fold point of the curve in the (k, b) -plane.

Remark 5.2. *The condition $A_{kb} \neq 0$ is generic. To see this, set up a moving orthonormal frame on the (k, b) curve. The tangent and a normal vectors are*

$$\mathbf{t}(s) = \frac{1}{\ell(s)} \begin{pmatrix} k'(s) \\ b'(s) \end{pmatrix} \quad \text{and} \quad \mathbf{n}(s) = \frac{1}{\ell(s)} \begin{pmatrix} b'(s) \\ -k'(s) \end{pmatrix},$$

with $\ell(s) = \sqrt{k'(s)k'(s) + b'(s)b'(s)}$. The gradient of $A_k(k, b)$, now considered as a field on (k, b) space, in the direction of \mathbf{n} at $s = s^*$, is

$$\mathbf{n} \cdot \nabla A_k = \frac{1}{\ell(s)} \begin{pmatrix} b'(s) \\ -k'(s) \end{pmatrix} \cdot \begin{pmatrix} A_{kk} \\ A_{kb} \end{pmatrix} = -\frac{1}{\ell} k'(s) A_{kb} \Big|_{s=s^*}.$$

Hence, with $k'(s^*) \neq 0$, A_{kb} is proportional to the normal derivative of A_k . Now, the curve (5.3) is the zero level set of $A_k(k, b)$ and, in the direction normal to that curve, the level sets on each side are generically non-zero level sets. It is in this sense that $A_{kb}(k(s^*), b(s^*)) \neq 0$.

The above approach appears to be the simplest strategy for finding the $A_k = A_{kk} = 0$ codimension two points. However, such codimension two points can be identified in other ways using different parameter spaces. Indeed, the most straightforward way is to compute A_{kk} along the curve (5.4), using the formula for A_{kk} in equation (A-3) in Appendix A, and monitor when it passes through zero. Interestingly, this strategy, when followed in the (A, b) -plane, produces a cusp at the codimension two point, so the point is easily identified.

The algorithm that implements Lemma 5.1 is based on solving the system

$$L(k)\hat{u} + f(\hat{u}) + cu_z = 0, \quad (5.5a)$$

$$L(k)\hat{u}_k + L'(k)\hat{u} + f'(\hat{u})\hat{u}_k + c_k\hat{u}_{kz} = 0, \quad (5.5b)$$

$$A_k(\hat{u}, \hat{u}_k) = 0 \quad (5.5c)$$

for $(\hat{u}, \hat{u}_k, c, c_k)$ and an additional equation parameter (e.g. b) on $z \in [0, 2\pi]$ along with periodic boundary conditions and phase conditions

$$\int_0^{2\pi} u_z^{\text{old}}(u - u^{\text{old}}) dz = \int_0^{2\pi} u_z^{\text{old}}(u_k - u^{\text{old}}) dz = \int_0^{2\pi} u_z^{\text{old}}(u_{kk} - u^{\text{old}}) dz = 0.$$

This allows us to continue curves of periodic orbits where $A_k = 0$ and one can then look for a cusp as another equation parameter is varied. Once the cusp point is located, we then add two more equations,

$$\begin{aligned} L(k)u_{kk} + 2L'(k)u_k + L''(k)u + f'(u)u_{kk} + f''(u)(u_k)^2 + c_{kk}(u_{kk})_z &= 0, \\ L(k)u_{kkk} + 3L'(k)u_{kk} + L''(k)u + 3L''(u)u_k + f'(u)u_{kkk} + f'''(u)u_k^3 + 3f''(u)u_ku_{kk} + c_{kkk}(u_{kkk})_z &= 0, \\ A_{kk}(u, u_k, u_{kk}) &= 0, \end{aligned}$$

for $(u_{kk}, u_{kkk}, c_{kk}, c_{kkk})$ with a further two phase conditions similar to the above, and another equation parameter (in this case, either μ or a), in order to trace out two parameter diagrams where $A_k = A_{kk} = 0$. Figure 12 shows the result of this computation, where a is treated as a continuation parameter for the fixed value $\mu = 0.3$. These codimension two curves emanate from the red dot shown in the pane of Fig. 11, i.e. the values of b and k are given when $a = 1.5$. In Figure 12(b), we indicate two points on the branch of codimension 2 curves, $p_{1,2}$. The action, $A(k)$, is computed near these codimension 2 points, and this computation is shown in panel 12(c). In this panel, the dashed curves are the plot of the action near p_1 and the solid curve is the plot of the action near p_2 .

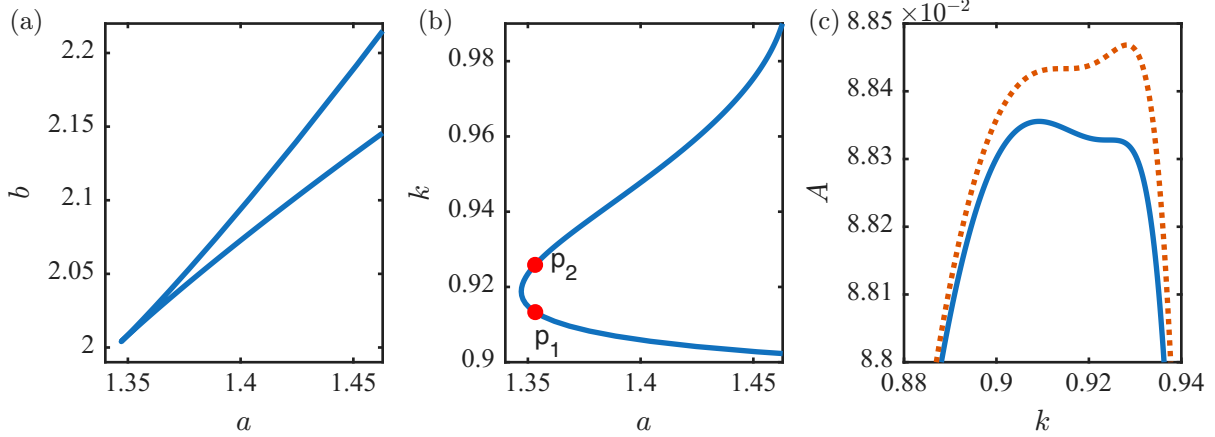


Figure 12: (a),(b) Parameter space for the SH357 equation (5.1) with $\mu = 0.3$ at which codimension 2 points occur. (c) Plot of the action, $A(k)$, near the points p_1 and p_2 labeled in panel (b), the dashed curve is near the point p_1 and the solid curve is near p_2 .

We now further probe the parameter space near the codimension two points. We summarize these results in Figure 13, where we plot an example of the Hamiltonian (1.3) as a function of k . Figure 13(a) shows the structure of the Hamiltonian as the coefficient of the cubic term, a , is varied. The value of $b = 2.15$ is fixed, and is chosen to coincide with the values obtained from the parameter continuation in Figure 12. The curve with parameter values near the codimension-two point is shown in black, while the curves of other colors have only slight changes in the parameter values. The relatively small parameter range for which such points exist illustrates the careful computational approach outlined in this section. Figure 13(b) is a zoom in of the small boxed region from panel (a) to illustrate the coalescence and annihilation of the critical points of the Hamiltonian as the parameters are varied.

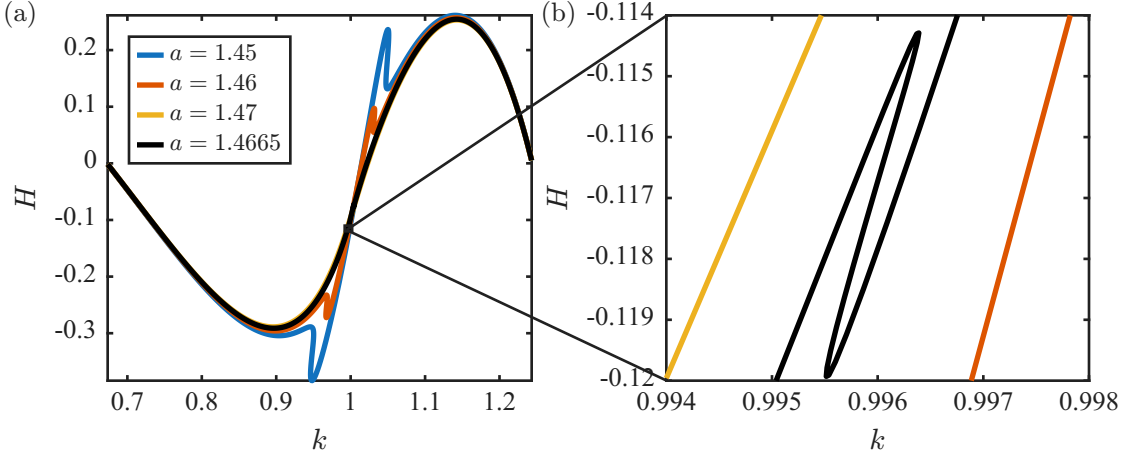


Figure 13: Behavior of the spatial Hamiltonian near the codimension 2 point for the SH357 equation with $\mu = 0.3$ and $a = 1.45$.

5.2 Heteroclinic connections near codimension two points

In this section, we will outline how we compute the connecting fronts emanating from the codimension two point found in §5.1. Given the discussion on the dimension of the intersection of the unstable and stable manifolds of the periodic orbits in §2.1, there are some choices in the set up the numerical methods in terms of which asymptotic parameters we wish to select. In particular, we need to find two parameters from the set $(k_-, k_+, \phi_-, \phi_+)$ if we do not use the Hamiltonian restriction. In what follows, we briefly outline a numerical implementation of the far-field core decomposition for the connecting fronts. The context will be general PDE systems whose connecting fronts select two parameters and then we describe how one adapts this for the conservative case.

We consider (1.1) in the abstract form

$$L(\partial_x)u + N(u) = 0, \quad (5.6)$$

where L is a linear and N a nonlinear operator. The proposed far-field core decomposition of $u(x)$ is

$$u(x) = u_-(k_-x + \phi_-)\chi_-(x) + w(x) + u_+(k_+x + \phi_+)\chi_+(x), \quad (5.7)$$

where $w(x)$ is the remainder function and $u_{\pm}(z)$ are periodic orbits satisfying

$$L(k_{\pm}\partial_z)u_{\pm} + N(u_{\pm}) + c_{\pm}(u_{\pm})z = 0, \quad u_{\pm}(z + 2\pi) = u_{\pm}(z), \quad \int_0^{2\pi} u_z^{\text{old}}(u_{\pm} - u^{\text{old}})dz = 0. \quad (5.8)$$

Upon substituting (5.7) into equation (1.1) we find an equation for the core $w(x)$ given by

$$Lw + \left(w + \sum_{\pm} u_{\pm}\chi_{\pm} \right) - \sum_{\pm} (Lu_{\pm} + N(u_{\pm}))\chi_{\pm} = 0. \quad (5.9)$$

We solve this equation on a large finite domain $x \in [-L, L]$, and add two phase conditions

$$\int_{\pm x=L-2\pi/k_{\pm}}^L w(x) \cdot \partial_x u_{\pm}(x; k_{\pm}, \phi_{\pm}) dx = 0. \quad (5.10)$$

In summary, we solve (5.8), (5.9) and (5.10) for fixed (k_-, ϕ_-) and $(u_{\pm}, w, k_+, \phi_+)$ if we wish to fix the value of the Hamiltonian level set, or we fix the phases (ϕ_-, ϕ_+) and solve for (u_{\pm}, w, k_{\pm}) .

Remark 5.3. *In order to restrict to a Hamiltonian level set, the integral condition for u_- is changed to the Hamiltonian constraint. This will restrict the periodic orbits to a specified Hamiltonian level set (i.e. this selects a k_-) and we then also fix ϕ_- . Either way, the two periodic orbits and the core will lie on some Hamiltonian level set.*

Numerically, we discretize the equations for u_{\pm} via a Fourier pseudo-spectral method [52] and use fourth-order finite differences for the w equation. They are implemented in MATLAB, and numerical continuation is implemented using AVITABILE ET AL. [2].

Based on the computation shown in Figure 12, we seek a heteroclinic connection in the unfolding of the codimension two point by selecting the parameters

$$\mu = 0.3, \quad a = 1.45, \quad b = 2.15.$$

A front is then computed between two periodic orbits by fixing the phases at the left and right ends of the domain (set to zero) and solve for the wavenumbers while varying a to approach the Hamiltonian codimension 2 point at $a \approx 1.466$. In Figure 14, we plot the result of this front computation in Panel (b). In Panel (a) we show that the wave numbers converge to the same value as we get close to the co-dimension 2 point.

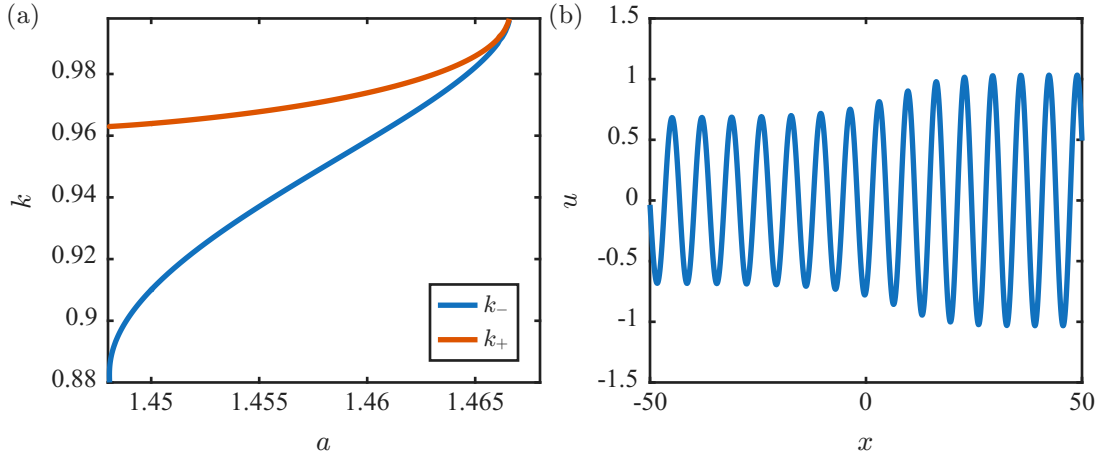


Figure 14: Wavenumber of the two periodic orbits in (a) as a function of the parameter a , coalescing at the codimension two point ($a \approx 1.466$). The right panel (b) shows a connecting orbit at $a = 1.45$ between two distinct periodic orbits in the unfolding of the codimension two point.

In summary, we have established an algorithm for finding a codimension two point in a field of periodic solutions, and have shown how heteroclinic connections are found in the unfolding of the codimension two point, as predicted by the normal form theory. In the next section we apply this strategy to a different PDE.

6 Fronts near codimension-two points in a Boussinesq system

The purpose of this section is three-fold: to show another example where a codimension two point can be found, to study a system that does not reduce to the SH form (1.1), and to compute oscillatory fronts in a Boussinesq system for the first time. The strategy is to first reduce the Boussinesq system (1.24) to a steady system on \mathbb{R}^4 , identify the Lagrangian, Hamiltonian, and action functionals, find a family of periodic orbits, and then implement our algorithm for zooming in on a codimension two point.

Relative to a moving frame, $x \mapsto x - Ct$, (1.24) is

$$-Ch_x + (u + hf'(u))_x + au_{xxx} = 0 \quad \text{and} \quad -Cu_x + f(u)_x + gh_x + ch_{xxx} = 0. \quad (6.1)$$

Integrating once, and using the function $F(h, u)$ defined in (1.27), it reduces to the conservative system on \mathbb{R}^4 ,

$$ch_{xx} = F_h \quad \text{and} \quad au_{xx} = F_u. \quad (6.2)$$

The Lagrangian and Hamiltonian densities for this system are

$$L = \frac{1}{2}au_x^2 + \frac{1}{2}ch_x^2 + F(h, u) \quad \text{and} \quad H = \frac{1}{2}au_x^2 + \frac{1}{2}ch_x^2 - F(h, u). \quad (6.3)$$

The equations (6.2) can be expressed as a canonical Hamiltonian system, but the structure won't be needed here, just the key invariants. The action density, for an ensemble of solutions, $h(x, s), u(x, s)$ parameterized by $s \in \mathbb{R}$, is

$$A = au_x u_s + ch_x h_s. \quad (6.4)$$

It satisfies the action conservation law

$$\frac{\partial A}{\partial x} = \frac{\partial L}{\partial s}. \quad (6.5)$$

When h, u are periodic in s , the integral of A over s is a relative integral invariant.

To compute codimension 2 points in the *ac*–Boussinesq system (1.24), we follow a similar approach to that outlined in Section 5.1 for the Swift-Hohenberg equation (1.1). For these computations, we fix the constants of integration to be $\mathcal{A} = -2$ and $\mathcal{B} = 2$, and set $C = 0$. The periodic orbits of wavenumber k are denoted by

$$u = \hat{u}(z, k) \quad h = \hat{h}(z, k) \quad z = kz, \quad (6.6)$$

and they satisfy the equations

$$ak^2\hat{u}_{zz} + \hat{u} + \hat{h}(\hat{u} + \alpha\hat{u}^2) = -2 \quad \text{and} \quad ck^2\hat{h}_{zz} + \hat{h} + \frac{1}{2}\hat{u}^2 + \frac{\alpha}{3}\hat{u}^3 = +2. \quad (6.7)$$

The action of this family of periodic orbits is

$$A(k) = \frac{1}{2\pi} \int_0^{2\pi} (ak\hat{u}_z^2 + ck\hat{h}_z^2) dz. \quad (6.8)$$

The codimension two point occurs when $A_k = A_{kk} = 0$ (equivalently $H_k = H_{kk} = 0$).

Periodic solutions are computed on the domain $z \in [0, 2\pi]$, and gradients with respect to k are computed using an approach similar to that in Section 5.1. Codimension 2 points are found by solving for values of k and α such that $A_k = A_{kk} = 0$ for fixed values of the dispersion coefficients a and c . For the sake of this computation, we will fix values of $c < 0$ and treat a as a continuation parameter.

In Figure 15, we show the continuation of the co-dimension 2 point for various values of c as a is varied. In panel (a), we show the wavenumber at the codimension 2 point, and in panel (b) the corresponding selected α value. We plot the spatial Hamiltonian near the co-dimension 2 point for $a = 0.2$ and $c = -0.3$ in the third panel of Figure 15. The geometry of the $H - k$ plot is similar to that in the SH357 equation in the previous section.

To compute the fronts, that emerge from the codimension two bifurcation point, we fix the phase of the far-field periodic orbits to be zero, and solve for the wavenumbers of the far-field periodic orbits. This strategy was also used in some of the SH357 calculations. The fronts in this case are computed using the farfield-core decomposition.

To find the codimension-two point, the strength of the highest order nonlinearity, α , is incremented until we reach a codimension 2 point at $\alpha \approx 0.1946$. At the codimension 2 point, the two wavenumbers coalesce to $k = k_- = k_+ \approx 2.12$. The wavenumbers of the far-field periodic orbits are shown in Fig. 16(a) as a function of α . We show a representative front solution near the codimension-two point with $\alpha = 0.194$ in Fig. 16(b) and (c). For this computation, the phase of the periodic solutions are fixed to be zero. For illustrative purposes, we show a similar family of PtoP solutions in Fig. 17, where the phase of the periodic orbit near $+\infty$ is fixed to be -0.25 .

Remark 6.1. *For the case of water waves ($\alpha = 0$ in the nonlinearity), the strategy would be to continue the family of fronts from $\alpha \approx 0.194$ down to $\alpha = 0$. On the other hand, there are models in the theory of water waves where the higher-order nonlinearity occurs, an example being the Boussinesq equations that have been derived at the interface between two fluids of different densities (e.g. Nguyen & Dias [37]).*

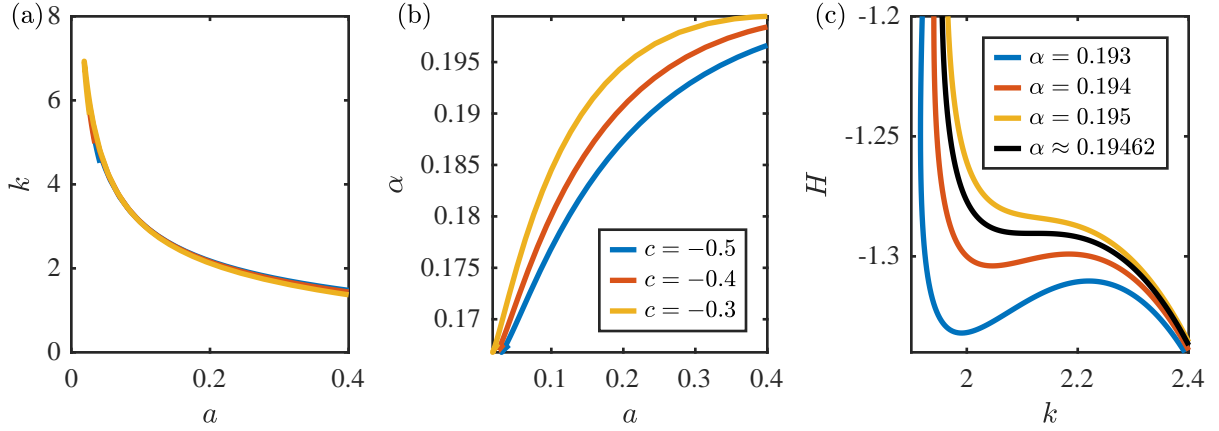


Figure 15: (a), (b) Parameter values for codimension two points for the steady ac-Boussinesq equation (6.7). (c) Spatial Hamiltonian near the codimension two point with $a = 0.2$ and $c = -0.3$ for various α showing the emergence of the codimension two point.

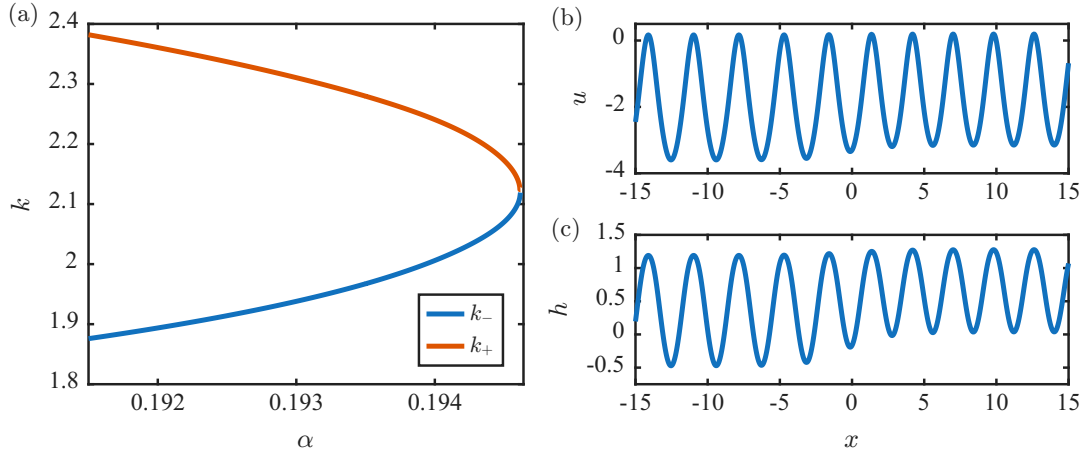


Figure 16: (a) Wavenumber of the far-field orbits that comprise the front solution of the ac-Boussinesq equation with $a = 0.2$ and $c = -0.3$ that bifurcate from the codimension two point. Panels (b) and (c) show two representative fronts near the codimension two point with $\alpha \approx 0.194$.

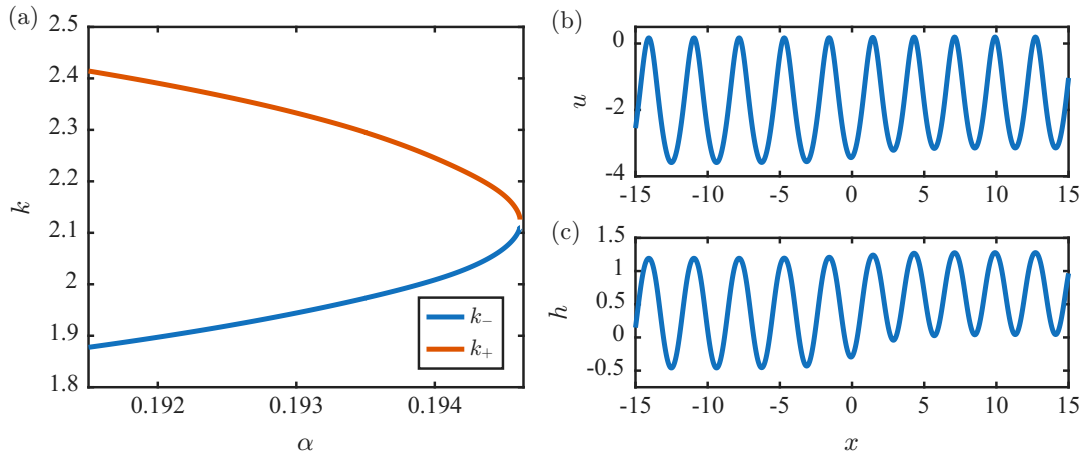


Figure 17: Same as Fig. 16, where the phase of the periodic orbit at $+\infty$ is fixed to -0.25 .

7 Concluding remarks

In this paper, we have clarified the geometric structure of PtoP heteroclinic connections in conservative systems in 4 phase space dimensions. This viewpoint makes it clear how the asymptotic phases are selected and why it is crucial to compute them in order to find heteroclinic connections and establish multiplicity. Moreover, it points to the geometry of the (un)stable manifolds as tubes, at least in the hyperbolic case (in contrast to the inverse hyperbolic). These observations build on extensions of previous work. We have taken the subject in a new direction by introducing the role of action, in both the numerics and in the normal form theory, and demonstrated the theory with examples. The above results point to a number of new directions.

Dimension counting. In phase space dimension greater than 4, dimension counting can be used to ascertain whether there will be selection of the asymptotic phases. For instance, in the 4D case, we can see the left periodic orbit has a 3-dimensional unstable manifold (coming from the two unit Floquet multipliers and one unstable multiplier) with corresponding co-dimension = $4 - 3 = 1$. The right periodic orbit has a 3-dimensional stable manifold (coming from the two unit Floquet multipliers and one stable multiplier) with corresponding co-dimension = $4 - 3 = 1$. The sum of the co-dimensions is 2. Hence, the dimension of the intersection is given by the dimension of the phase space minus the sum of the co-dimensions, i.e. $4 - 2 = 2$ and so we need two parameters to be selected for the intersection to occur. Since the periodic orbits have to lie in the same Hamiltonian level set, for a given left periodic orbit with a fixed wavelength and phase, there will be a selected wavelength of the right periodic orbit due to the Hamiltonian, leaving the phase of the right periodic orbit to be selected as part of the intersection. This dimension counting argument carries over to phase space dimension 6 and higher. Indeed, some intriguing results on heteroclinic connections between both periodic orbits and quasiperiodic (QP) tori, in a 6-dimensional phase space, have been reported in BARESI ET AL. [6] and OWEN & BARESI [38], with the latter showing that knot theory can be used to determine multiplicity of QP connections.

Action and normal form. A key contribution of the paper is the unfolding of the coalescence of two hyperbolic periodic orbits using modulation theory, resulting in the generic asymptotic equation (4.5). This equation introduces a new and important quantity, the Action, for the understanding of the heteroclinic connections in Hamiltonian systems. The advantage of the modulation equation is that it helps one find where such heteroclinic connections will occur just by understanding the geometric properties of the periodic orbit at the coalescence point. While this asymptotic equation is universal, it unfortunately does not provide any information on the phase selection process at the codimension two point or the unfolding. We suspect this would require going beyond-all orders asymptotics. We have also described a systematic numerical method for locating the coalescence point and shown that this coalescence point occurs in two different systems. Hence, we believe this organizing center to be common.

Space-time normal form. Going back to the normal form (1.15), and including a slow time $T = \varepsilon^4 t$, while also adding u_t to (1.1), results in a time-dependent modulation equation, which is a Cahn-Hilliard equation,

$$q_T = (\mathcal{K} q_{XX} + \frac{1}{6} A_{kkk} q^3)_{XX}. \quad (7.1)$$

The Cahn-Hilliard equation has been derived before using phase modulation by Düll [19] for a class of reaction-diffusion equations. In that case, the nonlinearity in the normal form was quadratic. The advantage of the cubic nonlinearity is that it generates fronts in the normal form. A complete analysis of this time-dependent PDE is outside the scope of this paper. However, we do point to two directions of interest. This equation could be used to get a first approximation to the stability of the fronts found in the normal form in §4.1. From results in the literature on stability of fronts of the Cahn-Hilliard equation (e.g. BRICMONT ET AL. [11]), there is reason to be optimistic that the fronts found in §4.1 will be stable. However this stability would be for the core only, and does not take into account the stability of the states at infinity. There is also reason to be optimistic that the time-dependent equation (7.1) will be valid, in the sense that solutions of it will stay close to solutions of the time-dependent SH equation. Düll [19] proves the validity of the quadratic Cahn-Hilliard equation, when compared with solutions of a coupled reaction-diffusion equation.

Inverse hyperbolic periodic orbits. As shown in Figure 9, there two cases of hyperbolic Floquet multipliers.

In this paper we have focused on the positive case. The negative case (inverse hyperbolic) appeared in Figure 6, but only in the third disconnected periodic orbit. The inverse hyperbolic case needs to be treated differently. For example, the unstable manifold is not orientable and has the structure of a Möbius band (e.g. Section 5 of MEISKE & SCHNEIDER [35] and Section 3 of AOUGAB ET AL. [1]). It is possible to connect hyperbolic and inverse hyperbolic periodic orbits by a heteroclinic in phase space dimension four, but the codimension two singularity here (coalescence of two periodic orbits) and associated normal form does not extend to coalescence of a hyperbolic and inverse-hyperbolic orbit, as a higher phase space dimension would be required.

Symplectic geometry. Periodic orbits in Hamiltonian systems have a Maslov index. There are several definitions of Maslov index in the literature (e.g. LONG [31]) and some definition will be operational here. Hence, an open question is the significance of the value of the Maslov index of each periodic orbit, or the difference between the two. Another open question is the significance of the value of the asymptotic phases or the jump in value when crossing the surface of section. Does it have a symplectic or other characterization?

Multi-space dimension PDEs. Looking ahead, the methods presented in this paper can, in principle, be extended to PDEs in two space dimensions; for example, to 2D hexagon fronts on the infinite periodic strip. The 2D hexagon front asymptotics, should carry through in the similar fashion to locate “stressed” hexagon connections and might explain the numerical investigations found on the plane [50]. The normal form theory can also capture, in principle, the coalescence of two hexagonal states. Most of the numerical methods for finding the coalescence point and the far-field core method carry over to 2 space dimensions as well; see for instance [29, 30]. From an asymptotic point of view, the more interesting case is the quasi-periodic connection set up (for both ODEs in higher space dimension, as noted above, and for PDEs [49]), where there would be multiple ‘Actions’ occurring. Unfolding that setup is likely to lead to new insights. Coalescence of two QP invariant tori can also be captured in a normal form. This direction would build on the important results of OWEN & BARESI [38]. Finally, it would be interesting to extend this theory to spatio-temporal wave train defects in Hamiltonian systems; that is, a multisymplectic version of [46, 45].

Data availability statement

The data that support the findings of this study are openly available at [13].

Acknowledgments

TB, DR, and PS would like to thank the Isaac Newton Institute for Mathematical Sciences for support and hospitality during that programme *Dispersive Hydrodynamics*, held in Autumn 2022, supported by EPSRC Grant Number EP/R014604/1, where this work was initiated. The authors are grateful to Michael Shearer for many helpful discussions on the project during that programme. The work of DL was partially supported by EPSRC Grant UKRI070. TB and DL are grateful to Nicola Baresi (Surrey Space Centre) for illuminating discussions about related work in astrodynamics. DR and PS are grateful to Surrey Mathematics for funding visits to work on the project. For the purpose of Open Access, the authors have applied a Creative Commons Attribution (CC BY) public copyright licence to any Author Accepted Manuscript version arising from this submission.

— Appendix —

A k –Derivatives of the action

In this appendix, we record formulas for the k –derivatives of the action functional evaluated on a family of periodic orbits. For reference, the formula for $A(k)$ is

$$A = \frac{1}{2\pi} \int_0^{2\pi} (\sigma k \hat{u}_z^2 - 2k^3 \hat{u}_{zz}^2) dz. \quad (\text{A-1})$$

The derivatives A_k , A_{kk} and A_{kkk} are obtained by direct calculation, so we just record the results. The first derivative is

$$A_k = \frac{1}{2\pi} \int_0^{2\pi} (\sigma \hat{u}_z^2 + 2\sigma k \hat{u}_z \hat{u}_{zk} - 6k^2 \hat{u}_{zz}^2 - 4k^3 \hat{u}_{zz} \hat{u}_{zzk}) dz. \quad (\text{A-2})$$

Differentiating a second time, and amalgamating terms

$$\begin{aligned} A_{kk} = & \frac{1}{2\pi} \int_0^{2\pi} (4\sigma \hat{u}_z \hat{u}_{zk} + 2\sigma k \hat{u}_{zk}^2 + 2\sigma k \hat{u}_z \hat{u}_{zkk} - 12k \hat{u}_{zz}^2 \\ & - 24k^2 \hat{u}_{zz} \hat{u}_{zzk} - 4k^3 \hat{u}_{zz} \hat{u}_{zzk} - 4k^3 \hat{u}_{zz} \hat{u}_{zzkk}) dz. \end{aligned} \quad (\text{A-3})$$

Differentiate a third time and simplify to get

$$\begin{aligned} A_{kkk} = & \frac{1}{2\pi} \int_0^{2\pi} (6\sigma \hat{u}_{zk}^2 + 6\sigma \hat{u}_z \hat{u}_{zkk} + 6\sigma k \hat{u}_{zk} \hat{u}_{zkk} + 2\sigma k \hat{u}_z \hat{u}_{zzkk} \\ & - 12\hat{u}_{zz}^2 - 72k \hat{u}_{zz} \hat{u}_{zzk} - 36k^2 \hat{u}_{zzk}^2 - 36k^2 \hat{u}_{zz} \hat{u}_{zzkk} \\ & - 12k^3 \hat{u}_{zzkk} \hat{u}_{zzk} - 4k^3 \hat{u}_{zz} \hat{u}_{zzkk}) dz. \end{aligned} \quad (\text{A-4})$$

All of the k –derivatives of A are quadratic in \hat{u} , and can be expressed using the inner product. For example,

$$A = \sigma k \langle \hat{u}_z, \hat{u}_z \rangle - 2k^3 \langle \hat{u}_{zz}, \hat{u}_{zz} \rangle.$$

The inner product representation will be important in the normal form theory.

B Derivation of the Nonlinear Normal Form

In this section, we will sketch the derivation of the normal form for the emergence of a heteroclinic connection near the co-dimension two point, $A_k = A_{kk} = 0$, using phase modulation.

Phase modulation for ODEs can be carried out using normal form transformations (e.g. Iooss [22], Mielke [36]). For PDEs, normal form transformations are cumbersome and therefore an ansatz approach is used (e.g. Doelman, et al. [17]). For conservative systems, phase modulation for PDEs is based on Whitham modulation theory which is built on an average Lagrangian (e.g. Bridges [12]). Here, we use the ansatz approach even for ODEs, as it is easier and will easily extend to the PDE case when we add in time and derive the Cahn-Hilliard equation (cf. §7). We will bring in the role of action *a posteriori*.

The derivation of the normal form, as mentioned in the main text of the paper, is achieved by substitution of the ansatz (4.1) into (1.1), expanding it in a Taylor series in ε , and solving order by order. At zeroth order we just recover the equation for the periodic solution, shifted in phase

$$k^4 \hat{u}_{zzzz}(z + \phi, k) + \sigma k^2 \hat{u}_{zz}(z + \phi, k) + V'(\hat{u}(z + \phi, k)) = 0. \quad (\text{B-1})$$

At first order, we find

$$\mathbf{L}(0)\hat{u}_k + 4k^3\hat{u}_{zzzz} + 2\sigma k\hat{u}_{zz} = 0,$$

where $\mathbf{L}(0)$ is defined in (3.14). This equation is satisfied exactly since it is just the derivative of (B-1) with respect to k . At second order, we find

$$\mathbf{L}(0)w_2 + q_X (4k^3\hat{u}_{zzzzk} + 6k^2\hat{u}_{zzz} + 2\sigma k\hat{u}_{zk} + \sigma\hat{u}_z) = 0.$$

The solvability condition for this equation is that the term proportional to q_X should be orthogonal to \hat{u}_z ,

$$0 = \langle \hat{u}_z, 4k^3\hat{u}_{zzzzk} + 6k^2\hat{u}_{zzz} + 2\sigma k\hat{u}_{zk} + \sigma\hat{u}_z \rangle.$$

Remarkably this solvability condition is precisely $A_k = 0$. This result is confirmed by differentiating

$$A(k) = \frac{1}{2\pi} \int_0^{2\pi} (\sigma k\hat{u}_z^2 - 2k^3\hat{u}_{zz}^2) dz.$$

The derivatives of $A(k)$ are recorded in Appendix A. The Jordan chain theory from §3.1 gives that the second order solution is $w_2 = q_X\xi_3 + c_2\xi_1$ where c_2 is an arbitrary constant.

At third order, after some calculation we find

$$\mathbf{L}(0)\left(w_3 - (\xi_3)_k q q_X - \xi_4 q_{XX}\right) = 0,$$

which is trivially solvable with solution,

$$w_3 = (\xi_3)_k q q_X + \xi_4 q_{XX} + c_3\xi_1,$$

where c_3 is an arbitrary constant.

The solvability condition at fourth order is what generates the normal form. The complete fourth order equation is

$$\mathbf{L}(0)w_4 + \Upsilon q^2 q_X + \mathcal{T} q_{XXX} + \mathbf{Solv} = 0, \quad (\text{B-2})$$

where \mathbf{Solv} are terms that vanish identically in the solvability condition, and the two key coefficients are

$$\begin{aligned} \Upsilon &= 2k^3\hat{u}_{zzzzkk} + 15k^2\hat{u}_{zzzzk} + 24k\hat{u}_{zzzz} + 4k^3(\xi_3)_{zzzzk} \\ &\quad + 6\hat{u}_{zzz} + 6k^2(\xi_3)_{zzzz} \\ &\quad + \sigma k\hat{u}_{zkkk} + \frac{1}{2}\sigma\hat{u}_{zk} + 2\sigma\hat{u}_{zk} + 2\sigma k(\xi_3)_{kzz} + \sigma(\xi_3)_{zz} \\ &\quad + \frac{1}{2}V''''(\hat{u})\hat{u}_k^2\xi_3 + \frac{1}{2}V''''(\hat{u})\hat{u}_{kk}\xi_3 + V''''(\hat{u})\hat{u}_k(\xi_3)_k, \end{aligned}$$

and

$$\mathcal{T} = 4k^3(\xi_4)_{zzz} + 2\sigma k(\xi_4)_z + 6k^2(\xi_3)_{zz} + \sigma\xi_3 + 4k\hat{u}_{zk} + \hat{u}_z.$$

Applying the solvability condition then gives

$$\mathcal{K} q_{XXX} + \kappa q^2 q_X = 0,$$

with

$$\begin{aligned} \kappa &= \langle \hat{u}_z, 2k^3\hat{u}_{zzzzkk} + 15k^2\hat{u}_{zzzzk} + 24k\hat{u}_{zzzz} + 4k^3(\xi_3)_{zzzzk} \\ &\quad + 6\hat{u}_{zzz} + 6k^2(\xi_3)_{zzzz} \\ &\quad + \sigma k\hat{u}_{zkkk} + \frac{1}{2}\sigma\hat{u}_{zk} + 2\sigma\hat{u}_{zk} + 2\sigma k(\xi_3)_{kzz} + \sigma(\xi_3)_{zz} \\ &\quad + \frac{1}{2}V''''(\hat{u})\hat{u}_k^2\xi_3 + \frac{1}{2}V''''(\hat{u})\hat{u}_{kk}\xi_3 + V''''(\hat{u})\hat{u}_k(\xi_3)_k \rangle. \end{aligned}$$

The other coefficient \mathcal{K} is

$$\mathcal{K} = \langle \hat{u}_z, \mathcal{T} \rangle = \langle \hat{u}_z, 4k^3(\xi_4)_{zzz} + 2\sigma k(\xi_4)_z + 6k^2(\xi_3)_{zz} + \sigma\xi_3 + 4k\hat{u}_{zk} + \hat{u}_z \rangle.$$

The major challenge is now to prove that $\kappa = \frac{1}{2}A_{kkk}$ and this is given in Appendix C. The parameter \mathcal{K} can be interpreted various ways: it can be related to the condition for termination of the Jordan chain in (3.18), or characterized in terms of derivatives of the Bloch coefficient (see Appendix D).

C Proof that 2κ equals A_{kkk} in normal form

In this appendix the proof is sketched that the coefficient of $q^2 q_X$ in the normal form, denoted by κ , can be expressed in terms of A_{kkk} . Details are in the supplementary material. Formulas for A and A_{kkk} are given in Appendix A.

Denote by Υ the vector-valued coefficient of $q^2 q_X$ in the ε^4 equation (see equation (B-2)),

$$\begin{aligned}\Upsilon = & 2k^3 \hat{u}_{zzzkkk} + 15k^2 \hat{u}_{zzzkk} + 24k \hat{u}_{zzzk} + 6 \hat{u}_{zzz} \\ & + 4k^3 (\xi_3)_{zzzzk} + 6k^2 (\xi_3)_{zzzz} + 2\sigma k (\xi_3)_{kzz} + \sigma (\xi_3)_{zz} \\ & + \sigma k \hat{u}_{zkkk} + \frac{5}{2} \sigma \hat{u}_{zkk} \\ & + \frac{1}{2} V''''(\hat{u}) \hat{u}_k^2 \xi_3 + \frac{1}{2} V'''(\hat{u}) \hat{u}_{kk} \xi_3 + V''(\hat{u}) \hat{u}_k (\xi_3)_k.\end{aligned}$$

Applying the solvability condition, the scalar-valued coefficient $\langle\langle \hat{u}_z, \Upsilon \rangle\rangle$ of $q^2 q_X$ is then

$$\begin{aligned}\kappa = & \langle\langle \hat{u}_z, 2k^3 \hat{u}_{zzzkkk} + 15k^2 \hat{u}_{zzzkk} + 24k \hat{u}_{zzzk} + 6 \hat{u}_{zzz} \\ & + \sigma k \hat{u}_{zkkk} + \frac{5}{2} \sigma \hat{u}_{zkk} \\ & + 4k^3 (\xi_3)_{zzzzk} + 6k^2 (\xi_3)_{zzzz} + 2\sigma k (\xi_3)_{kzz} + \sigma (\xi_3)_{zz} \\ & + \frac{1}{2} V''''(\hat{u}) \hat{u}_k^2 \xi_3 + \frac{1}{2} V'''(\hat{u}) \hat{u}_{kk} \xi_3 + V''(\hat{u}) \hat{u}_k (\xi_3)_k \rangle\rangle.\end{aligned}$$

The aim is to show that $2\kappa = A_{kkk}$, where A_{kkk} is given in Appendix A. We note that A_{kkk} is a quadratic functional and can therefore be written in terms of the inner product. This will be useful when comparing it with the form of κ . The inner product based expression for A_{kkk} , evaluated on a family of periodic orbits, is

$$\begin{aligned}A_{kkk} = & 6\sigma \langle\langle \hat{u}_{zk}, \hat{u}_{zk} \rangle\rangle + 6\sigma \langle\langle \hat{u}_z, \hat{u}_{zkk} \rangle\rangle + 6\sigma k \langle\langle \hat{u}_{zk}, \hat{u}_{zkk} \rangle\rangle + 2\sigma k \langle\langle \hat{u}_z, \hat{u}_{zkkk} \rangle\rangle \\ & - 12 \langle\langle \hat{u}_{zz}, \hat{u}_{zz} \rangle\rangle - 72k \langle\langle \hat{u}_{zz}, \hat{u}_{zzk} \rangle\rangle - 36k^2 \langle\langle \hat{u}_{zzk}, \hat{u}_{zzk} \rangle\rangle - 36k^2 \langle\langle \hat{u}_{zz}, \hat{u}_{zkkk} \rangle\rangle \\ & - 12k^3 \langle\langle \hat{u}_{zkkk}, \hat{u}_{zzk} \rangle\rangle - 4k^3 \langle\langle \hat{u}_{zz}, \hat{u}_{zkkk} \rangle\rangle.\end{aligned}\tag{C-1}$$

In A_{kkk} are k and z derivatives of \hat{u} , whereas in κ we find terms with ξ_3 as well as derivatives with respect to z and k of ξ_3 . Starting with the Jordan chain equation for ξ_3 and differentiating, we find equations for ξ_3 , $(\xi_3)_k$, $(\xi_3)_z$, and so on. Back substituting all these equations, integrating by parts, and simplifying gives the result. The details are in the supplementary material.

D Connection between \mathcal{K} and the Bloch spectrum

This appendix is concerned with connecting the coefficient of the spatial derivative with a quantity that can be computed independently of the asymptotic analysis, which transpires to be the Bloch spectrum of the original wavetrain \hat{u} . To observe this, we follow previous work on phase dynamics [17, 43] and construct the Bloch spectral problem for (1.1):

$$\mathbf{L}(\nu) = (i\nu + k\partial_z)^4 + \sigma (i\nu + k\partial_z)^2 + V''(\hat{u})\tag{D-1}$$

Whilst the main paper focuses on the Goldstein mode to this operator (i.e. exactly at $\nu = 0$), we will instead consider the generalization where the operator admits a continuous spectrum near zero:

$$\mathbf{L}(\nu)W(z, \nu) = \mu(\nu)W(z, \nu).\tag{D-2}$$

Here we assume the eigenvalue $\mu(\nu)$ is at least 4 times differentiable in the neighborhood of $\nu = 0$. The relationship between the Bloch spectrum $\mu(\nu)$ and \mathcal{K} is established by taking ν -derivatives and relating these derivatives to inner products of the basic wave. Since $\mathbf{L}(0)$ and the original system are invariant under $z \rightarrow -z$ transformations,

it follows that the Bloch spectrum should also be invariant under $\nu \rightarrow -\nu$ transformations. This leads to the observation that the spectrum $\mu(\nu)$ is an even function of ν , so $\mu'(0) = \mu'''(0) = 0$. Furthermore, $\mathbf{L}(0)$ is self adjoint. Finally, given the coincidence of $\mathbf{L}(0)$ with the linear operator of the original system extracted from a z derivative of (1.1) we have that $\mu(0) = 0$ and $W(z, 0) = \hat{u}_z$. This means that \hat{u}_z is also the adjoint eigenfunction by assumption.

We now seek a relationship between μ and the basic state. The first derivative of (D-2) evaluated at zero gives

$$\mathbf{L}(0)\partial_\nu W(z, 0) = \mu'(0)\hat{u}_z - \mathbf{L}'(0)\hat{u}_z = -(4k^3\hat{u}_{zzzz} + 2k\sigma\hat{u}_{zz}),$$

where the primes herein denote differentiation with respect to ν . Comparisons to a k derivative of the equation for the basic state and the above expression shows that

$$\partial_\nu W(z, 0) = i\hat{u}_k.$$

Taking a second derivative of (D-2) and evaluating it at zero gives the next order problem:

$$\mathbf{L}(0)\partial_\nu^2 W(z, 0) = \mu''(0)\hat{u}_z - 2i\mathbf{L}'(0)\hat{u}_k - \mathbf{L}''(0)\hat{u}_z = \mu''(0)\hat{u}_z + 8k^3\hat{u}_{zzzz} + 4k\sigma\hat{u}_{zk} + 12k^2\hat{u}_{zzz} + 2\sigma\hat{u}_z.$$

This system is solvable, which is required as is its the derivative of a strict equality, when the right hand side vanishes under the inner product established in the main paper. We can see that

$$\begin{aligned} \mu''(0) &= -\frac{\langle\langle \hat{u}_z, 8k^3\hat{u}_{zzzz} + 4k\sigma\hat{u}_{zk} + 12k^2\hat{u}_{zzz} + 2\sigma\hat{u}_z \rangle\rangle}{\langle\langle \hat{u}_z, \hat{u}_z \rangle\rangle} \\ &= -\frac{1}{2\pi\langle\langle \hat{u}_z, \hat{u}_z \rangle\rangle} \int_0^{2\pi} 2\sigma\hat{u}_z^2 + 4\sigma\hat{u}_z\hat{u}_{zk} - 12k^2\hat{u}_{zz}^2 - 8k^3\hat{u}_{zz}\hat{u}_{zzk} dz = -\frac{2A_k}{\langle\langle \hat{u}_z, \hat{u}_z \rangle\rangle}. \end{aligned}$$

We note that the denominator here can be removed by redefining $W(z, 0) = \hat{u}_z/\langle\langle \hat{u}_z, \hat{u}_z \rangle\rangle$. The condition assumed in the main paper is that $A_k = 0$, meaning this derivative of μ vanishes and thus the equation at this order is solvable with

$$\partial_\nu^2 W(z, 0) = -2\xi_3.$$

This will be the final parts of our analysis. A third derivative, with all our previous results, gives

$$\mathbf{L}\partial_\nu^3 W(z, 0) = -[\mathbf{L}'''(0)\hat{u}_z + 3i\mathbf{L}''(0)\hat{u}_k - 3\mathbf{L}'(0)\xi_3]$$

which from the main paper gives that $\partial_\nu^3 W(z, 0) = -6i\xi_4$. One final derivative gives our final order, where the key result emerges:

$$\begin{aligned} \mathbf{L}\partial_\lambda^4 W(z, 0) &= \mu^{(4)}(0)\hat{u}_z - [\mathbf{L}''''(0)\hat{u}_z + 4i\mathbf{L}'''(0)\hat{u}_k - 6\mathbf{L}''(0)(2\xi_3) - 4i\mathbf{L}'(0)(6\xi_4)] \\ &= \mu^{(4)}(0)\hat{u}_z - 24[\hat{u}_z + 4k\hat{u}_{zk} + (6k^2\partial_{zz} + \sigma)\xi_3 + (4k^3\partial_z^3 + 2\sigma k\partial_z)\xi_4] \end{aligned}$$

Imposing solvability and using the definition of \mathcal{K} gives our desired result:

$$\mu'''(0) = \frac{24\mathcal{K}}{\langle\langle \hat{u}_z, \hat{u}_z \rangle\rangle},$$

with the observation that one can again remove the denominator by redefining $W(z, 0)$.

E Underpinning symplectic geometry

The properties and implications of action become clearer when the symplectic structure of the governing equations is revealed. We already showed that the first-order form (1.4) is Hamiltonian with a non-canonical symplectic operator

\mathbf{J} , defined in (1.5). We now transform the coordinates (u_1, u_2, u_3, u_4) to canonical (q_1, q_2, p_1, p_2) via

$$\begin{pmatrix} q_1 \\ q_2 \\ p_1 \\ p_2 \end{pmatrix} = \begin{bmatrix} 1 & 0 & 0 & 0 \\ 0 & 0 & 1 & 0 \\ 0 & \sigma & 0 & 1 \\ 0 & 1 & 0 & 0 \end{bmatrix} \begin{pmatrix} u_1 \\ u_2 \\ u_3 \\ u_4 \end{pmatrix}.$$

This transformation, denoted by \mathbf{T} is symplectic in the sense that $\mathbf{T}^T \mathbf{J}_C \mathbf{T} = \mathbf{J}$, where \mathbf{J}_C is the canonical symplectic operator

$$\mathbf{J}_C := \begin{bmatrix} 0 & 0 & -1 & 0 \\ 0 & 0 & 0 & -1 \\ 1 & 0 & 0 & 0 \\ 0 & 1 & 0 & 0 \end{bmatrix}.$$

The first-order form (1.4) is then transformed to

$$-\mathbf{p}_x = \partial_{\mathbf{q}} H \quad \text{and} \quad \mathbf{q}_x = \partial_{\mathbf{p}} H, \quad (\text{E-1})$$

with Hamiltonian function,

$$H(\mathbf{q}, \mathbf{p}) = p_1 p_2 - \frac{\sigma}{2} p_2^2 - \frac{1}{2} q_2^2 + V(q_1).$$

In canonical coordinates, the action is based on the one form $\mathbf{p} \cdot d\mathbf{q}$. Let $(\mathbf{q}(x, s), \mathbf{p}(x, s))$ be solutions of (E-1) parameterized by s and 2π -periodic in s , as in (3.6). Then

$$\frac{d}{dx} \oint \mathbf{p} \cdot \mathbf{q}_s \, ds = 0,$$

which can be confirmed by direct calculation. This is in fact the Poincaré-Cartan theorem, which can be found in most textbooks on Hamiltonian dynamics. Figure 8 shows a schematic of the theorem in action. Back substituting for \mathbf{q} and \mathbf{p} ,

$$p_1(q_1)_s + p_2(q_2)_s = (u_4 + \sigma u_2)(u_1)_s + u_2(u_3)_s = (u_{xxx} + \sigma u_x)u_s + u_x u_{xxs},$$

recovering the definition of action in (3.6).

A second result which becomes clearer in the Hamiltonian setting is the formula $H_k = kA_k$ proved in Lemma 3.1. Here it will follow from a constrained variational principle. Let $z = kx$ and substitute into (E-1), giving

$$\underbrace{k \begin{bmatrix} \mathbf{0} & -\mathbf{I} \\ \mathbf{I} & \mathbf{0} \end{bmatrix} \begin{pmatrix} \mathbf{q} \\ \mathbf{p} \end{pmatrix}}_{\nabla A} \Big|_z = \underbrace{\begin{pmatrix} \partial_{\mathbf{q}} H \\ \partial_{\mathbf{p}} H \end{pmatrix}}_{\nabla H}, \quad (\text{E-2})$$

In other words, 2π -periodic solutions can be characterized as critical points of H on level sets of the action, with k as Lagrange multiplier, and (E-2) as the Lagrange necessary condition; that is, $\nabla H = k \nabla A$. Given a solution of this variational principle, it follows that

$$H_k = \langle\langle \nabla H, U_k \rangle\rangle = \langle\langle \nabla H - k \nabla A, U_k \rangle\rangle + k \langle\langle \nabla A, U \rangle\rangle = kA_k,$$

on solutions, with $U := (\mathbf{q}, \mathbf{p})$, giving a concise proof of Lemma 3.1, where $\langle\langle \cdot, \cdot \rangle\rangle$ is an inner product for 2π -periodic vector valued functions, generalizing (3.17).

Since the system (E-1) is first order, the Jordan chain theory of §3 is for the linear eigenvalue problem

$$[D^2 H - k D^2 A] \mathbf{v} = \lambda \mathbf{J}_C \mathbf{v}.$$

The left-hand side has a symmetric operator and the right-hand side has a skew-symmetric operator. The Jordan chain, for an eigenvalue λ_* satisfies

$$\mathbf{L} \mathbf{v}_{j+1} = \lambda_* \mathbf{J}_C \mathbf{v}_{j+1} + \mathbf{J} \mathbf{v}_j, \quad j = 1, 2, \dots, \quad \text{with } \mathbf{L} = D^2 H - k \mathbf{J}_C \frac{d}{dz}.$$

In the symplectic setting, other new variational characterizations appear. For example, in the case of SH357, all the parameters in H appear linearly, and so it can be split into a sum of functionals

$$H(\mathbf{q}, \mathbf{p}) = H_0 - \mu H_1 - a H_2 - b H_3.$$

In this case the Lagrange necessary condition, generalizing (E-2), is

$$\nabla H_0 = k \nabla A + \mu \nabla H_1 + a \nabla H_2 + b \nabla H_3,$$

with k, μ, a, b now considered as Lagrange multipliers. However, we have not as yet found any advantage to this more general variational principle.

The symplectic form of the equations also simplifies the phase modulation. For example, without any structure, the formula relating A_{kkk} to the normal form coefficient κ in Appendix C is quite surprising. Using symplectic phase modulation (e.g. Bridges [12]), it can be reduced to a few terms. Indeed, we did the calculation first from a symplectic viewpoint and then transformed coordinates to apply to the setting of the scalar-valued ODE (1.1).

References

- [1] AOUGAB, T., BECK, M., CARTER, P., DESAI, S., SANDSTEDE, B., STADT, M., AND WHEELER, A. Isolas versus snaking of localized rolls. *J. Dynam. Differential Equations* 31, 3 (2019), 1199–1222.
- [2] AVITABILE, D. Numerical Computation of Coherent Structures in Spatially-Extended Systems. Zenodo. doi: 10.5281/zenodo.3821169.
- [3] BANDARA, R., GIRALDO, A., BRODERICK, N. G. R., AND KRAUSKOPF, B. Generalized and multi-oscillation solitons in the nonlinear Schrödinger equation with quartic dispersion. *Chaos* 33, 7 (2023), 073154.
- [4] BANDARA, R. I., GIRALDO, A., BRODERICK, N. G. R., AND KRAUSKOPF, B. Infinitely many multipulse solitons of different symmetry types in the nonlinear Schrödinger equation with quartic dispersion. *Phys. Rev. A* 103, 6 (2021), 063514.
- [5] BANDARA, R. I., GIRALDO, A., BRODERICK, N. G. R., AND KRAUSKOPF, B. Bifurcations of periodic orbits in the generalised nonlinear Schrödinger equation. *J. Comput. Dyn.* 12, 2 (2025), 178–211.
- [6] BARESI, N., OLIKARA, Z. P., AND SCHEERES, D. J. Fully numerical methods for continuing families of quasi-periodic invariant tori in astrodynamics. *J. Astro. Sci.* 65, 2 (2018), 157–182.
- [7] BARRABÉS, E., MONDELO, J. M., AND OLLÉ, M. Numerical continuation of families of heteroclinic connections between periodic orbits in a Hamiltonian system. *Nonlinearity* 26, 10 (2013), 2747–2765.
- [8] BECK, M., KNOBLOCH, J., LLOYD, D. J. B., SANDSTEDE, B., AND WAGENKNECHT, T. Snakes, ladders, and isolas of localized patterns. *SIAM J. Math. Anal.* 41, 3 (2009), 936–972.
- [9] BEYN, W.-J. On well-posed problems for connecting orbits in dynamical systems. In *Chaotic numerics (Geelong, 1993)*, vol. 172 of *Contemp. Math.* Amer. Math. Soc., Providence, RI, 1994, pp. 131–168.
- [10] BONA, J. L., CHEN, M., AND SAUT, J.-C. Boussinesq equations and other systems for small-amplitude long waves in nonlinear dispersive media. II. The nonlinear theory. *Nonlinearity* 17, 3 (2004), 925–952.
- [11] BRICMONT, J., KUPIAINEN, A., AND TASKINEN, J. Stability of Cahn-Hilliard fronts. *Comm. Pure Appl. Math.* 52, 7 (1999), 839–871.
- [12] BRIDGES, T. J. *Symmetry, Phase Modulation and Nonlinear Waves*, vol. 31. Cambridge University Press, 2017.

[13] BRIDGES, T. J., LLOYD, D. J. B., RATLIFF, D. J., AND SPRENGER, P. *Heteroclinic_PtoP_1D*, 2026. Github repository, https://github.com/David-JB-Lloyd-Lab/Heteroclinics_PtoP_1D.

[14] BRONSKI, J. C., HUR, V. M., AND JOHNSON, M. A. Modulational instability in equations of KdV type. In *New approaches to nonlinear waves*. Springer, 2016, pp. 83–133.

[15] DIECI, L., AND REBAZA, J. Point-to-periodic and periodic-to-periodic connections. *BIT* 44, 1 (2004), 41–62.

[16] DOEDEL, E. J., KOOI, B. W., VAN VOORN, G. A. K., AND KUZNETSOV, Y. A. Continuation of connecting orbits in 3D-ODEs. II. Cycle-to-cycle connections. *Internat. J. Bifur. Chaos* 19, 1 (2009), 159–169.

[17] DOELMAN, A., SANDSTEDE, B., SCHEEL, A., AND SCHNEIDER, G. *The dynamics of modulated wave trains*. American Mathematical Society, 2009.

[18] DRISCOLL, C., AND O’NEIL, T. Modulational instability of cnoidal wave solutions of the modified Korteweg–de Vries equation. *Journal of Mathematical Physics* 17, 7 (1976), 1196–1200.

[19] DÜLL, W.-P. The validity of phase diffusion equations and of Cahn–Hilliard equations for the modulation of pattern in reaction-diffusion systems. *J. Diff. Eqns.* 239, 1 (2007), 72–98.

[20] HENRY, D., AND SCHEERES, D. A survey of heteroclinic connections in the earth-moon system. In *Proc. 73rd Inter. Astro. Congress, Paris* (2022), pp. 1–12.

[21] HOYLE, R. B. *Pattern Formation: an Introduction to Methods*. Cambridge University Press, 2006.

[22] IOOSS, G. Global characterization of the normal form for a vector field near a closed orbit. *Journal of Differential Equations* 76, 1 (1988), 47–76.

[23] KAHEMAN, K., BRAMBURGER, J. J., KUTZ, J. N., AND BRUNTON, S. L. Saddle transport and chaos in the double pendulum. *Nonlinear Dynamics* 111, 8 (2023), 7199–7233.

[24] KAMCHATNOV, A., KUO, Y.-H., LIN, T.-C., HORNG, T.-L., GOU, S.-C., CLIFT, R., EL, G., AND GRIMSHAW, R. H. Undular bore theory for the Gardner equation. *Physical Review E* 86, 3 (2012), 036605.

[25] KIRCHGRABER, U., AND STOFFER, D. Possible chaotic motion of comets in the Sun–Jupiter system—a computer-assisted approach based on shadowing. *Nonlinearity* 17, 1 (2004), 281–300.

[26] KNOBLOCH, E., UECKER, H., AND WETZEL, D. Defectlike structures and localized patterns in the cubic-quintic-septic Swift–Hohenberg equation. *Phys. Rev. E* 100, 1 (2019), 012204.

[27] KNOBLOCH, J., AND RIESS, T. Lin’s method for heteroclinic chains involving periodic orbits. *Nonlinearity* 23, 1 (2010), 23–54.

[28] KOON, W. S., LO, M. W., MARSDEN, J. E., AND ROSS, S. D. Heteroclinic connections between periodic orbits and resonance transitions in celestial mechanics. *Chaos* 10, 2 (2000), 427–469.

[29] LLOYD, D. J. Hexagon invasion fronts outside the homoclinic snaking region in the planar Swift–Hohenberg equation. *SIAM J. Appl. Dyn. Syst.* 20, 2 (2021), 671–700.

[30] LLOYD, D. J. B., AND SCHEEL, A. Continuation and bifurcation of grain boundaries in the Swift–Hohenberg equation. *SIAM J. Appl. Dyn. Syst.* 16, 1 (2017), 252–293.

[31] LONG, Y. *Index theory for symplectic paths with applications*, vol. 207 of *Progress in Mathematics*. Birkhauser Verlag, Basel Switzerland, 2002.

[32] LÓPEZ-GÓMEZ, J., AND MORA-CORRAL, C. *Algebraic multiplicity of eigenvalues of linear operators*, vol. 177 of *Operator Theory: Advances and Applications*. Birkhäuser Verlag, Basel, 2007.

- [33] MADDOCKS, J. H. Stability and folds. *Arch. Rational Mech. Anal.* **99**, 4 (1987), 301–328.
- [34] MAGNUS, R. J. A generalization of multiplicity and the problem of bifurcation. *Proc. London Math. Soc.* (3) **32**, 2 (1976), 251–278.
- [35] MEISKE, W., AND SCHNEIDER, K. Topological structure of integral manifolds and period-doubling bifurcation. *Zeit. Angew. Math. Phys.* **38** (1987), 302–314.
- [36] MIELKE, A. A spatial center manifold approach to steady bifurcations from spatially periodic patterns, in "Dynamics in Dissipative Systems: Reductions, Bifurcations and Stability" (by G. Dangelmayr, B. Fiedler, K. Kirchgässner and A. Mielke), Pitman Research Notes **352**, 1996.
- [37] NGUYEN, H. Y., AND DIAS, F. A Boussinesq system for two-way propagation of interfacial waves. *Physica D* **237** (2008), 2365–2389.
- [38] OWEN, D., AND BARESI, N. Applications of knot theory to the detection of heteroclinic connections between quasi-periodic orbits. *Astro dynamics* **8**, 4 (2024), 577–595.
- [39] PALMER, K. *Shadowing in dynamical systems*, vol. 501 of *Mathematics and its Applications*. Kluwer Academic Publishers, Dordrecht, 2000.
- [40] PAMPEL, T. Numerical approximation of connecting orbits with asymptotic rate. *Numer. Math.* **90**, 2 (2001), 309–348.
- [41] PAMPEL, T. Error estimates of a computational method for generalised connecting orbits. *Open Numer. Meth. J.* **1** (2009), 6–19.
- [42] RABIER, P. J. Generalized Jordan chains and two bifurcation theorems of Krasnoselskii. *Nonlinear Anal.* **13**, 8 (1989), 903–934.
- [43] RATLIFF, D. Genuine nonlinearity and its connection to the modified Korteweg–de Vries equation in phase dynamics. *Nonlinearity* **35**, 1 (2021), 30.
- [44] RATLIFF, D., TRICHTCHENKO, O., AND BRIDGES, T. Modulation leading to frequency downshifting of water waves in the vicinity of the Benjamin–Feir transition. *J. Fluid Mech.* **1014** (2025), A1–A23.
- [45] ROBERTS, T. V., AND SANDSTEDE, B. Homoclinic snaking of contact defects in reaction-diffusion equations. *Nonlinearity* **38**, 11 (2025), Paper No. 115001, 36.
- [46] SANDSTEDE, B., AND SCHEEL, A. Defects in oscillatory media: toward a classification. *SIAM J. Appl. Dyn. Syst.* **3**, 1 (2004), 1–68.
- [47] SPEAR, R., L. *Planar heteroclinic connections in the Neptune-Triton circular restricted three body problem*. PhD thesis, University of Colorado, 2021.
- [48] SPRENGER, P., BRIDGES, T. J., AND SHEARER, M. Traveling wave solutions of the Kawahara equation joining distinct periodic waves. *J. Nonlinear Sci.* **33**, 5 (2023), Paper No. 79, 39.
- [49] SUBRAMANIAN, P., ARCHER, A. J., KNOBLOCH, E., AND RUCKLIDGE, A. M. Three-dimensional icosahedral phase field quasicrystal. *Phys. Rev. Lett.* **117** (Aug 2016), 075501.
- [50] SUBRAMANIAN, P., ARCHER, A. J., KNOBLOCH, E., AND RUCKLIDGE, A. M. Snaking without subcriticality: grain boundaries as non-topological defects. *IMA J. Appl. Math.* **86**, 5 (2021), 1164–1180.
- [51] THOMPSON, J. Stability predictions through a succession of folds. *Phil. Trans. Roy. Soc. Lond. A* **292** (1979), 1–23.

- [52] TREFETHEN, L. N. *Spectral methods in MATLAB*, vol. 10 of *Software, Environments, and Tools*. Society for Industrial and Applied Mathematics (SIAM), Philadelphia, PA, 2000.
- [53] UECKER, H., WETZEL, D., AND RADEMACHER, J. pde2path – a Matlab package for continuation and bifurcation in 2d elliptic systems. *Numer. Math. Theor. Meth. Appl.* 7 (2014), 58–106.
- [54] WILCZAK, D., AND ZGLICZYSKI, P. Heteroclinic connections between periodic orbits in planar restricted circular three-body problem—a computer assisted proof. *Comm. Math. Phys.* 234, 1 (2003), 37–75.
- [55] WILCZAK, D., AND ZGLICZYSKI, P. Heteroclinic connections between periodic orbits in planar restricted circular three body problem. II. *Comm. Math. Phys.* 259, 3 (2005), 561–576.
- [56] ZHANG, W., KRAUSKOPF, B., AND KIRK, V. How to find a codimension-one heteroclinic cycle between two periodic orbits. *Discrete Contin. Dyn. Syst.* 32, 8 (2012), 2825–2851.